IMPLEMENTATION OF AN OFDM BASED UNDERWATER ACOUSTIC MODEM

A THESIS

SUBMITTED TO THE DEPARTMENT OF ELECTRICAL AND

ELECTRONICS ENGINEERING

AND THE GRADUATE SCHOOL OF ENGINEERING AND SCIENCES

OF BILKENT UNIVERSITY

IN PARTIAL FULFILLMENT OF THE REQUIREMENTS

FOR THE DEGREE OF

MASTER OF SCIENCE

By

Emrecan Demirörs

August 2011

I certify that I have read this thesis and that in my opinion it is fully adequate, in scope and in quality, as a thesis for the degree of Master of Science.

Prof. Dr. Hayrettin Köymen (Supervisor)

I certify that I have read this thesis and that in my opinion it is fully adequate, in scope and in quality, as a thesis for the degree of Master of Science.

Assist. Prof. Dr. Sinan Gezici

I certify that I have read this thesis and that in my opinion it is fully adequate, in scope and in quality, as a thesis for the degree of Master of Science.

Assist. Prof. Dr. Arif Sanlı Ergün

Approved for the Graduate School of Engineering and Sciences:

Prof. Dr. Levent Onural
Director of Graduate School of Engineering and Sciences

ABSTRACT

IMPLEMENTATION OF AN OFDM BASED UNDERWATER ACOUSTIC MODEM

Emrecan Demirörs
M.S. in Electrical and Electronics Engineering
Supervisor: Prof. Dr. Hayrettin Köymen
August 2011

In this thesis we designed and implemented an underwater acoustic (UWA) communication system employing multicarrier modulation in the form of orthogonal frequency division multiplexing (OFDM). UWA communication became more popular as there has been a growing interest in transmitting real-time data, such as video and sonar images. There are many applications where these transmissions are used. These applications are underwater wireless sensor networks(UWSN) and unmanned underwater vehicles (UUVs) for military and scientific purposes. Therefore, building an efficient UWA communication system which has a high data rate can improve these applications' performance significantly. Currently, many underwater communication systems use single carrier modulation which have limited data rate due to complexity of their receivers, as frequency selectivity of the channel increases when the symbol rate increases, so we preferred to use multicarrier modulation in UWA communication in order to increase data rate of our system. In this thesis, we considered a system that uses zero-padded (ZP) OFDM modulation. Based on ZP-OFDM, we used a receiver model that performs pilot-tone based channel estimation, carrier frequency offset compensation based on least squares (LS) fitting error or null subcarriers if they occur and data demodulation for each OFDM block individually. We used MATLAB environment for implementing our system. The MATLAB scripts generate a data burst that contains OFDM blocks, and then it is transmitted to the hardware from a laptop by using a Data Acquisition (DAQ) Card. At the other side of the system, the receiver laptop gets the data by using a DAQ Card. As the data is received, MATLAB scripts are used for demodulating it. As we built our system, we performed underwater experiments at Bilkent Lake Facility to investigate its performance in a real UWA channel. In our test, a data rate of 13.92 kbps has been achieved with quadrature phase shift keying (QPSK) modulation while the bit-error-rate (BER) was less then $9x10^{-2}$ without using any coding.

Keywords: Multicarrier modulation, orthogonal frequency division multiplexing (OFDM), underwater acoustic (UWA) communication

ÖZET

OFDM TABANLI BİR SUALTI AKUSTİK MODEMİNİN GERÇEKLENMESİ

Emrecan Demirörs
Elektrik ve Elektronik Mühendisliği Bölümü Yüksek Lisans
Tez Yöneticisi: Prof. Dr. Hayrettin Köymen
Ağustos 2011

Bu tezde, çok taşıyıcılı modülasyonu, dikey frekans bölmeli çoklama (OFDM) yapisinda kullanan bir sualtı akustik iletişim sistemi tasarlanmış ve yapılmıştır. Gerçek zamanlı veri, video ve sonar görüntüsü göndermeye artan ilgiden dolayı, sualtı akustik iletişimi daha popüler olmuştur. Bu aktarımlar, askeri ve bilimsel uygulamalarda kullanılan sualtı sensör ağları ve insansız sualtı araçları gibi bir çok uygulamada kullanılmaktadırlar. Bu nedenle, yüksek veri aktarım hızına sahip etkin bir sualtı akustik iletişim sistemi, bahsi geçen bu uygulamaların performanslarını önemli ölçüde geliştirebilir. Halizhazırda kullanılan bir çok iletişim sisteminde, alıcıların karmaşıklığından ötürü sınırlı veri aktarım hızına sahip olan tek taşıyıcılı modülasyon tekniği kullanılmaktadır. Bu karmaşıklığın sebebi, sembol aktarım hızı artıkça kanalın daha fazla frekans seçici sönümleme yapmasıdır. Bu nedenle biz veri aktarım hızını artırabilmek için, sualtı akustik iletişimde çok taşıyıcılı modülasyonu kullanmaya ve incelemeye karar verdik. Bu tezde, sıfır ile dolgulanmış (ZP)-OFDM modülasyonu incelenmiştir. ZP-OFDM'ye bağlı olarak kullanılan alıcı modeli, her OFDM bloğunda ayrı olmak üzere pilot-sembol destekli kanal kestirimi, en küçük karaler kestirimine veya eğer bulunuyorsa boş alt taşıyıcılara dayanan taşıyıcı frekans ofseti dengelemesi ve veri demodülasyonu yapmaktadır. Bu tezde, sistem gerçeklemesi için MATLAB ortamı kullanılmıştır. MATLAB kodları tarafından oluşturulan ve OFDM blokları içeren veri paketleri kullanılan veri edinme (DAQ) kartı ile bir dizüstü bilgisayardan donanıma aktırılır.

Sistemin diğer ucunda ise alıcı dizüstü bilgisayar bir veri edinme kartı sayesinde veriyi alır. Verinin alınması ile beraber, MATLAB kodları ile demodülasyon işlemi gerçekleştirilir. Bu şekilde tanımlanan sistemimizin gerçek bir sualtı ortamındaki performansını görmek için Bilkent Üniversitesi Gölet Tesisinde, sualtı deneyleri gerçekleştirilmiştir. Bu testler sonucunda, dördün faz kaydırmalı modülasyonunu kullanan ve herhangibir kodlama işlemi içermeyen sistemimiz, bit hata oranı $9x10^{-2}$ altında iken 13.92 kbps veri aktarım hızına ulaşmıştır.

Anahtar Kelimeler: Çok Taşıyıcılı modülasyon, dikey frekans bölmeli çoklama (OFDM), sualtı akustik iletişimi

Acknowledgements

I would like to express my sincere gratitude to my advisor, Prof. Dr. Hayrettin Köymen of the Electrical and Electronics Department at Bilkent University, for his advice, encouragement, enduring patience and constant support. He always provided clear explanations when I was lost, and always giving me his time, in spite of anything else that was going on. I wish all students the honor and opportunity to experience his ability to perform at that job.

I also want to thank the other members of my committee, Assist. Prof. Dr. Sinan Gezici of the Electrical and Electronics Department at Bilkent University. He has always supported me, and has given great advices since my undergraduate and helps me whenever I need. It was a great honor to be his student. I also want to thank Assist. Prof. Dr. Arif Sanlı Ergün Electrical and Electronics Department at TOBB University of Economy and Technology for his suggestions and comments that were invaluable to the completion of this work.

I want to thank to Electrical and Electronics Department professors and staff for all their hard work and dedication, providing me the means to complete my degree and prepare for an academic career. Especially, to Prof. Dr. Yusuf Ziya İder, Assoc. Prof. Dr. Ezhan Karaşan and Prof. Dr. Erdal Arıkan for their invaluable supports and helps.

I would like to thank Meteksan Defence Industry Inc., and my principles there who has given me support during my research, especially K. Selçuk Alparslan and Cihangir Duran.

I would like to thank my colleague Mine Merve Yüksel who helped me in the every part of my work. It was a great pleasure working with her. I would like to thank my colleagues Görkem Kar, M. Oğuzhan Saçma, M. Talha Işık, Alper Bereketli, H. Kağan Oğuz, A. Sinan Taşdelen for their discussions and comments in my research. I also want to thank my friends M. Arcan Ertürk, Efecan Poyraz, Sinan Yıldırım, Serdar Öğüt, Çağatay Güngör, Uğur Yıldız and Çağrı Uzunoğlu for their supports during my research process.

I am very grateful to my parents Ferda Özlem and Nejat Demirörs and my family who have always given me their unconditional caring and support.

Table of Contents

List of Figures

List of Tables

Chapter 1

INTRODUCTION

Underwater applications are used and needed in many areas such as military, fishing, research, oil and mine detection [1]. Underwater channels should be identified in order to be used. Today acoustic waves are the only effective way to establish underwater applications as radio waves are severely attenuated and optical waves suffer from scattering and need high precision. Acoustic waves can be used in underwater applications to detect and locate obstacles and targets, for measuring characteristics of the marine environment and for transmitting signals to provide wireless underwater communication.

In this thesis, we concentrate on the underwater acoustic (UWA) communications. As the attention on the underwater applications has increased, underwater communication systems received their share of interest. There has been a great growing interest in transmitting real-time data, video and sonar images. There are many applications where these transmissions are used like underwater wireless sensor networks(UWSN) for scientific research and military applications [2], [3] and unmanned underwater vehicles (UUVs) for military and scientific applications [4]. Therefore, building an efficient UWA communication system which has a high data rate can improve these applications' performance significantly.

Based on that idea, several UWA communication systems have been established. The most common ones are the coherent underwater communication systems that use single carrier modulation [5], [6]. However, these systems have limited data rate due to complexity of their receivers, as frequency selectivity of the channel increases when the symbol rate increases. Thus, a single carrier system cannot fulfill the high data rate requirement of underwater applications. In order to reach required high data rates, multicarrier modulation in the form of orthogonal frequency division multiplexing (OFDM) is proposed [7], [8].

Multicarrier modulation in the form of OFDM is established its success in wireless communications over radio channels. OFDM simplifies the receiver complexity, deals with multipath with its long symbol duration compared to multipath spread and can give great results even in highly dispersive radio channels. Thus, it has been used in many radio communication systems like wireless LAN(IEEE 802.11 a/g/n)[9], metropolitan area networks(IEEE 802.16, WiMAX) [10], [11] and wireless digital video broadcasting (DVB). This success motivates researchers to work on OFDM in underwater acoustic communication, as UWA channel is highly dispersive, frequency-selective and has a long multipath spread.

The research on OFDM in underwater acoustic communications has been simulation based or conceptual work [12], [13] , [14] until, Prof. Milica Stojanovic and her co-researchers proposed successful experimental results in [7] ,[8], [15]. In our work, we implemented our system based on the proposed algorithms and system models of Prof. Milica Stojanovic and her co-researchers in [7] ,[8], [15].

In this thesis, we built a UWA communication system that uses zero-padded ZP-OFDM modulation instead of cyclic prefixing (CP). The reason behind is that CP can spend too much transmission power and it is not so effective in underwater channels where long delay spread occurs [16]. Based on ZP-OFDM modulation, we built a transmitter and a receiver model. The transmitter model basically uses IFFT modulation method as we use rectangular pulse shaping. The transmitter also contains a mapping block which maps information bits into quadrature phase shift keying (QPSK) symbols. In addition to that, blocks that insert time synchronization preamble and make the zero-padding operation are present in the transmitter model. In our receiver model, we prefer a system that processes each OFDM block individually. The model contains a block that can perform carrier frequency offset compensation based on least squares (LS) fitting error or null subcarriers if they occur. Besides that, receiver performs a pilot-tone based channel estimation and data demodulation.

In this thesis, we use MATLAB environment for implementing our system. The MATLAB scripts generate a data burst that contains OFDM blocks, and then it is transmitted to the hardware from a laptop by using a Data Acquisition (DAQ) Card. At the other side of the system, the receiver laptop gets the data by using a DAQ Card. As the data is received, MATLAB scripts are used for demodulating it. As we build our system, we performed underwater experiments at Bilkent Lake Facility to investigate its performance in a real UWA channel. In our test, a data rate of 13.92 kbps has been achieved while the bit-error-rate (BER) was varied between 10^{-1} and 10^{-2} without using any coding.

The rest of the thesis is organized as follows: In Chapter 2, we introduce the underwater channel and its challenges. In Chapter 3, we introduce concept, use, advantages and disadvantages of orthogonal frequency-division multiplexing (OFDM). In Chapter 4, our transmitter design is proposed. In Chapter 5, our receiver design is proposed. In Chapter 6, the system deployment for underwater experiments are explained. In Chapter 7, results of underwater experiments are presented and analyzed. In Chapter 8, we summarize our conclusions.

Chapter 2

THE UNDERWATER CHANNEL

The most common way to send data in underwater environment is by means of acoustic signals. Dolphins and whales use it to communicate. Radio frequency signals have serious problems in sea water, and can only operate at very short ranges (up to 10 meters) and with low-bandwidth modems (terms of kbps). When using optical signals the light is strongly scattered and absorbed underwater, so only in very clear water conditions (often very deep) does the range go up to 100 meters with high bandwidth modems (several Mbps).

According to Urick [1], sound propagation is regular molecular movement in an elastic substance that propagates to adjacent particles. A sound wave can be considered as the mechanical energy that is transmitted by the source from particle to particle propagating through the ocean at the sound speed. The propagation of such waves will refract upwards or downwards in agreement with the changes in salinity, temperature and the pressure that have a great impact on the sound speed, ranging from 1450 to 1540 m/s.

As acoustic signals are mainly used in underwater communications, it is vital to characterize the major factors affecting acoustic propagation in underwater environments, where (1) low speed of sound introduces high latency and relatively large motion-induced Doppler effects; (2) phase and magnitude fluctuations lead to higher bit error rates compared with radio channels' behavior; (3) as propagation is best supported at low frequencies, acoustic communication systems are inherently wideband; (4) propagation underwater acoustic (UWA) communications over multiple paths. All these facts along with others put important implications on design structures.

2.1 Physical Layer: Acoustic Link

Transmision Loss(TL)is the loss in intensity level between two field points, generally referred to as the source and receiver. Factors contributing to TL is summarized below.

2.1.1 Attenuation

In UWA channels path loss depends on the signal frequency due to absorption. In addition to the absorption loss, signal experiences a spreading loss which increases with distance. The overall path loss occurs in an UWA channel for a signal of frequency f over a transmission distance l taken in reference to some l_r is given by the following equation:

$$A(l,f) = (l/l_r)^k a(f)^{l-l_r} \tag{2.1}$$

where k is the spreading factor, which describes the geometry of propagation , and $\alpha(f)$ is the absorption coefficient. Expressed in dB:

$$10 \log A(l,f) = k.10 \log(l/l_r) + (l - l_r).10 \log \alpha(f) \tag{2.2}$$

2.1.1.1 Spreading factor

Spreading loss is the TL due to the geometric spreading of acoustic energy as sound travels away from the source. Typically, the spreading loss depends only on range of propagation. Therefore, it is frequency independent(when point sources and targets are used). The two simplest models for spreading loss are spherical and cylindrical.

2.1.1.1.1 Spherical Spreading Spherical spreading occurs when an acoustic wave radiates spherically outward from the source in an unbounded medium. Spreading factor k becomes 2 for spherical spreading.

2.1.1.1.2 Cylindrical Spreading In the bounded medium that has the characteristic of a waveguide such as the ocean, which is bounded by the ocean surface and floor, acoustic waves travel outward between two parallel surfaces. Therefore, at ranges much greater than the depth, the energy propagates cylindrically. Spreading factor k becomes 1 for cylindrical spreading.

For practical spreading one can take k as 1.5.

At Bilkent Lake Facility, where we conducted our experiments, spherical spreading mainly occurs as the distance between receiver and transmitter is small, even the environment is bounded.

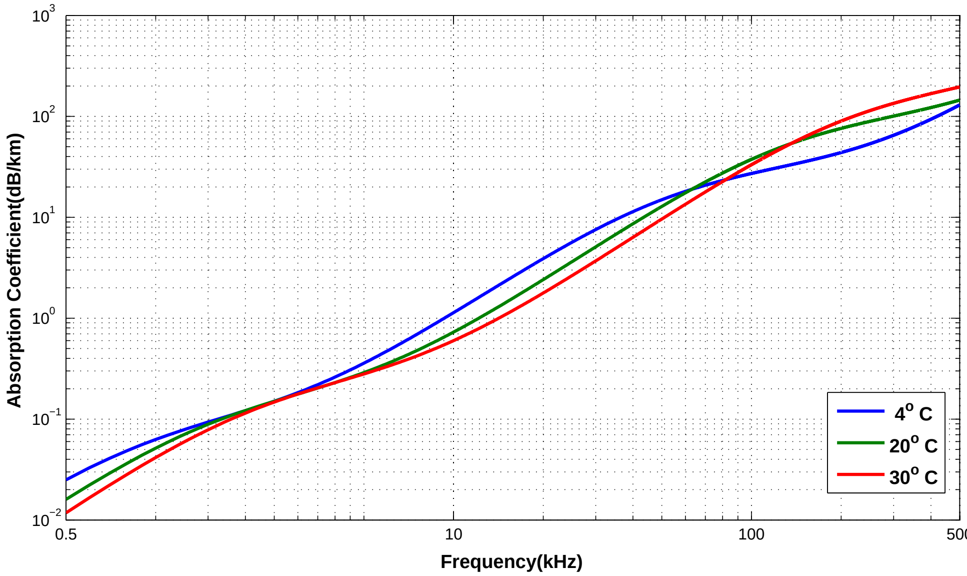

Figure 2.1: Absorption Coefficient

2.1.1.2 Absorption Coefficient

A second mechanism of signal loss results from the conversion of the energy in the propagating signal into heat. This mechanism is referred to as absorption loss. In sea water the absorption loss of acoustic signals is strongly frequency dependent and increases with frequency. Signal energy decay due to absorption loss is proportional to $\exp -\alpha(f)d$ where absorption coefficient $\alpha(f)$ is an increasing function of frequency and d is propagation distance.

The absorption coefficient for frequencies above a few hundred Hz can be expressed empirically, using the Thorp's formula [17] which gives $\alpha(f)$ in dB/km for f in kHz as in Eq. (2.3)

$$10 \log \alpha(f) = 0.11 \frac{f^2}{f^2+1} + 44 \frac{f^2}{f^2+4100} + 2.75 \cdot 10^{-4} f^2 + 0.003 \tag{2.3}$$

Absorption coefficient rapidly increases with frequency (see Fig.2.1), so the total path loss will also increase, so there is an upper limit for frequency usage.

Considering the points mentioned above, there are two factors that should be noted. First, at short ranges the spherical spreading loss dominates the absorption loss. Second, even at short ranges (e.g., approximately 400 meters) the absorption loss at 100 kHz exceeds that of 25 kHz by nearly 15 dB. The practical impact of the frequency dependence of absorption loss is that the communications channel is effectively band-limited and available bandwidth is a decreasing function of range. This characteristic can significantly impact choice of modulation and multi-access techniques.

2.1.2 Noise

There are several important sources of ambient noise in the ocean at frequencies of interest for acoustic communications. Ambient noise in the underwater communications channel originates from both natural and man-made sources. Naturally occurring noise is caused by biological and seismic activities and by hydrodynamic noise from waves, currents, tides, rain and wind. Man-made noise is mainly due to shipping activities. Contributions of each noise source can be described empirically based on formula provided by Coates [18].

$$10 \log N_t(f) = 17 - 30 \log f \tag{2.4a}$$

$$10 \log N_s(f) = 40 + 20(s - 5) + 26 \log f - 60 \log(f + 0.03) \tag{2.4b}$$

$$10 \log N_w(f) = 50 + 7.5w^1/2 + 20 \log f - 40 \log(f + 0.04) \tag{2.4c}$$

$$10 \log N_{th}(f) = -15 + 20 \log f \tag{2.4d}$$

where N_t is the due to turbulence, N_s is due to shipping, N_w is due to wind, and N_{th} represents the thermal noise. The overall noise power spectral density for a given frequency f is then:

$$N(f) = N_t(f) + N_s(f) + N_w(f) + N_{th}(f) \tag{2.5}$$

Fig. 2.2 shows the estimated Noise Spectrum Level (NSL) in deep water based on formula provided by Coates[18]. The NSL is generally dependent on four sources, each dominating certain frequency bands, namely trubulence ($< 10Hz$), shipping ($10-200Hz$), wind ($0.2-100kHz$) and thermal activity ($> 100kHZ$) [18]. Of course, these sources are variable depending on weather and other factors. The noise increases at the low frequency range, thus limiting the useful acoustic bandwidth from below.

However Coates' empirical formulas are based on data taken in deep water and do not include biological noise such as from snapping shrimp, whose noise signature is of high amplitude and wide bandwidth, and which can be found in many shallow-water environments.

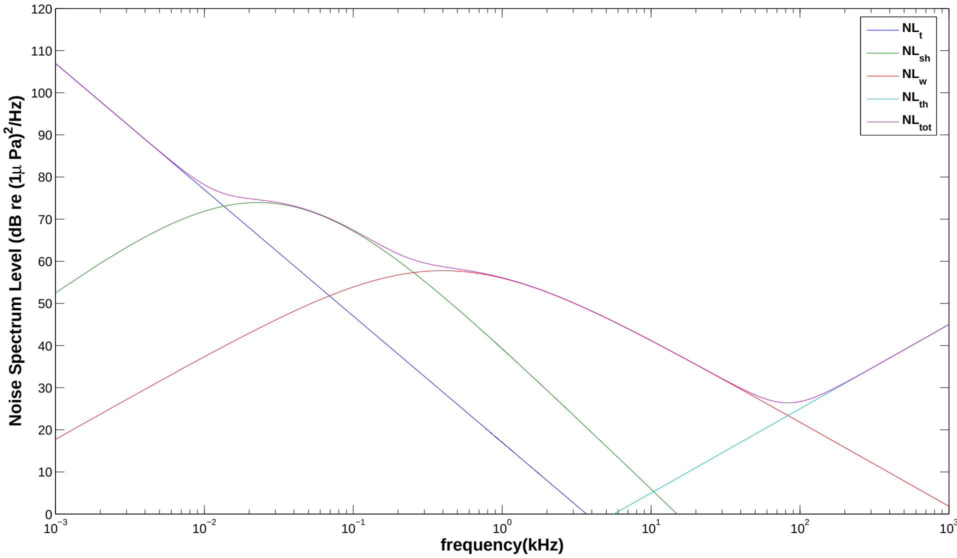

Figure 2.2: The noise spectrum level (NSL) in dB based on empirical formulas by Coates.

This noise is so effective on system performances that special researches are made on these environments [19].

In shallow water, noise is not as well defined as it is in deep water. This is because there is greater variability in both time and place in shallow water environments than in deep water. However, Urick states there are three major categories of noise in shallow water: wind noise, biological noise and shipping noise [1]. The combination of these three noise sources determines noise levels in shallow water.

For our experimental purposes, range is short and signal power is high, as a result we did not work in a noise-limited environment. However, depending on experimental setup and environmental conditions, one should take the above points into account.

2.1.3 The Fading Channel

2.1.3.1 Multipath Spread

Multipath sound propagation (reception) refers to situations in which there are additional sound transmission pathways in addition to direct path propagation.

In deep water and over long ranges, multipath reception by a receiver generally results from refractive propagation paths, as opposed to paths that include boundary reflections. In this case, cumulative boundary reflection losses, especially with the ocean bottom, effectively eliminate boundary multipath propagation from contributing to distant received acoustic signal. Multipath propagation due to boundary reflections suffers severe TL as bounce losses for long range propagation in the deep ocean accumulate. Therefore, the most important multipath contributors to distant received signals are only from refractive rays. In shallow water, at typical ranges of interest, multipath propagation from source to receiver is an important sound transmission pathway because, other than direct path propagation, there might only be one or two boundary reflected paths that contribute to a received signal. Therefore, the effect of these interactions must be considered and the boundaries of both surface and floor must be treated as potentially lossy reflectors. When an acoustic ray interacts with one of the boundaries, its signal characteristics, such as frequency, phase, and amplitude may change. Each ray travels with a unique path, as illustrated by Fig. 7.5 in Section 7.1.2. Each ray arriving at the receiver is called an eigenray. Since each eigenray has a unique path, it also has a unique arrival time. There is the possibility of constructive and destructive interferences due to different phases of rays arriving at the receiver at different arrival times. These interferences might cause severe fluctuation in transmission loss.

The time spread of a signal refers to the spreading out, in time, of the transmitted signal as it propagates to the receiver. As the multipath rays arrive at the receiver, the resulting received signal, when compared to the transmitted version of the signal, may appear to have spread in time. Thus, it may be said that multipath propagation lengthens the channel's impulse response, which in turn causes the received signal to spread in time. The time interval over which these multipath signals arrive at the receiver is called the multipath spread of the channel, and is denoted by T_m [20]. The multipath spread of the channel can be inversely represented in frequency by the coherence bandwidth of the channel give by [20].

$$\Delta f_c \approx \frac{1}{T_m} \tag{2.6}$$

If the bandwidth of the transmitted signal is greater than Δf_c , the channel is frequency selective. If the bandwidth of the transmitted signal is less than Δf_c , the channel is frequency-nonselective.

In our experiment, the channel is frequency selective as it is common for underwater acoustic channel(UWA).

2.1.3.2 Doppler Spread

The range of frequencies over which the Doppler power spectrum of the channel is nonzero is called the Doppler spread of the channel, and is denoted by B_d [20] . Doppler spread can be inversely represented in time by the coherence time of the channel, given by [20] :

$$\Delta t_c \approx \frac{1}{B_d} \tag{2.7}$$

If coherence time has a larger value than the delay constraints of the channel, it corresponds to a fast-fading channel. Else if it has smaller value than the delay constraints of the channel, it corresponds to a slow-fading channel. Doppler spread occurs as a result of Doppler shifts caused by motion at the source, receiver, and channel boundaries. Mobile nodes exhibit a Doppler shift proportional to their relative velocity, while currents and tides can also force moored nodes to move, introducing slight Doppler shifts. The boundaries can introduce Doppler shifts when rays interact with gravity waves; this is particularly evident at the surface, but can also occur in stratified water in which internal waves may be propagating.

In multipath propagation, a Doppler shift can occur every time a ray interacts with a boundary. Thus, the frequency observed at the receiver is a combination of all the various frequency shifts the signal has encountered through it's multipath propagation. These shifts contribute of the formation of the multipath-induced fading channel. Because the Doppler shift are velocity dependent, the more perturbed boundaries are, for instance due to a large sea state, the greater the Doppler shifts will be.

For stationary boundary conditions , reflections do not introduce Doppler shifts. The bandwidth of the Doppler spread is the accumulation of the total effects of motion at the source, receiver, and channel boundaries have on the frequency observed at the receiver. The spread refers to the tendency of a transmitted signal's bandwidth B to spread out in the frequency domain as it propagates through the fading channel. The bandwidth of the signal observed at the receiver may then be $B+\Delta B$, where ΔB is the additional bandwidth the received signal occupies as a result of propagation through a fading channel.

The frequency shift is mainly described by the factor $a = v_r/c$, where v_r is the relative velocity between transmitter and receiver, and c is the signal propagation speed (the speed of sound underwater in this case). In underwater environments c is much lower than electromagnetic waves, and so the Doppler effect is not ignorable. In addition, the fact that underwater systems are wideband causes much different Doppler shifts for different frequency components of the transmitted signal. Here, each frequency f_k is shifted by an amount that cannot be approximated as equal for all subcarriers as opposed to narrowband systems. As exaggerated view can be seen in Fig. 2.3. This non-uniform Doppler effect should be treated carefully.

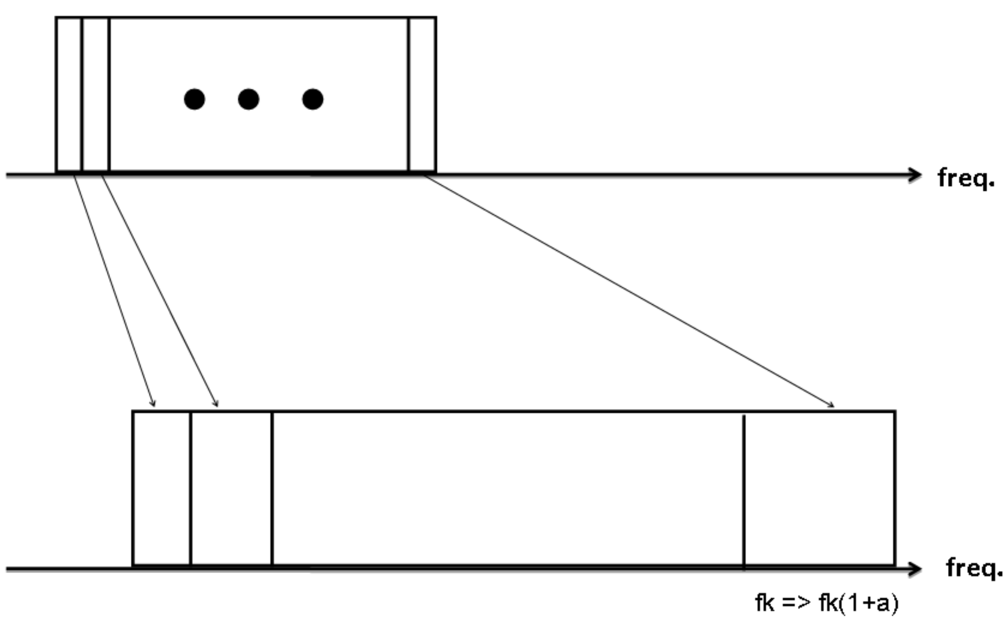

Figure 2.3: Motion-induced Doppler shift is not uniform in a wideband system.

2.1.3.3 Inter-symbol Interference

Inter-symbol interference (ISI) is a form of distortion of a signal in which one symbol interferes with subsequent symbols. This is an undesirable phenomenon, as the previous symbols have a similar effect as noise, thus making communications less reliable. ISI is usually caused by multipath spread of the inherent nonlinear frequency response of a channel, causing successive symbols to "blur" together. The presence of ISI in the system introduces errors in the decision device at the receiver output.

Fig. 2.4 shows a long-range source-receiver configuration. Shown are two eigenrays, the direct path and the surface-reflected path. The time difference of arrival between the two rays is depicted as pulse trains, and we see that, compared to the pulse duration T, this multipath spread T_m is relatively small, corresponding to relatively small overlap between symbols, and therefore low ISI. In Fig. 2.5, a short-range source-receiver configuration is shown. In this case, T_m is large compared to the pulse duration T, corresponding to relatively large overlap between symbols, and therefore more ISI. If T is shortened, the overlap becomes even greater.

2.1.4 Frequency Allocation

In contrast to the radio-frequency spectrum, the acoustic spectrum is not regulated (yet). However, taking into account the bandwidth limitations caused by the acoustic path loss and the ambient noise, the frequency allocation possibilities are not numerous.

2.1.4.1 The SNR

The narrowband signal-to-noise ratio (SNR), which is a dimensionless measure, is given by [21]

$$SNR(l,f) = \frac{S(f)\Delta f / A(l,f)}{N(f)\Delta f} = \frac{S(f)}{A(l,f)N(f)} \tag{2.8}$$

The factor where $S(f)$ is the power spectral density of the transmitted signal and Δf is a narrow frequency band around f. For each transmission distance , there exists an optimal frequency $f_o(l)$ for which the narrowband SNR is maximized. Note that this result

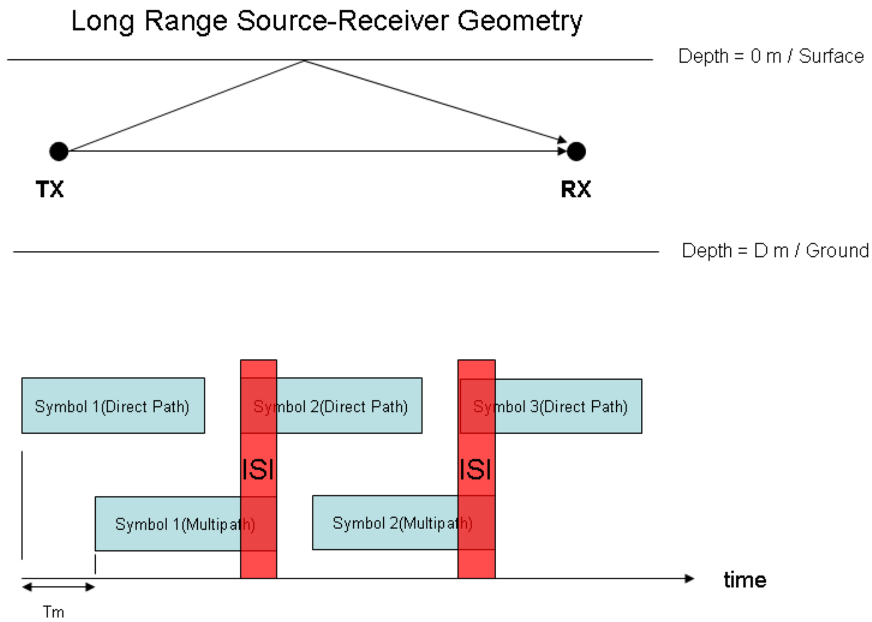

Figure 2.4: Direct-path and surface-reflected path pulse trains for a long-range source receiver geometry.

is invariant to the fixed noise p.s.d. level η_o . In practice, this level can include a margin to guarantee sufficient transmission power to close the link.

2.1.4.2 Bandwidth Definition

We define the 3-dB bandwidth below the maximum value of the $SNR(l, f)$, $B_{3dB}(l)$, in hertz, as the range of frequencies around $f_o(l)$ for which $A(l, f)N(f) < 2A(l, f_0(l)N(f_0(l))$. As the transmission distance is reduced, the optimal frequency increases and so does its corresponding 3-dB bandwidth.

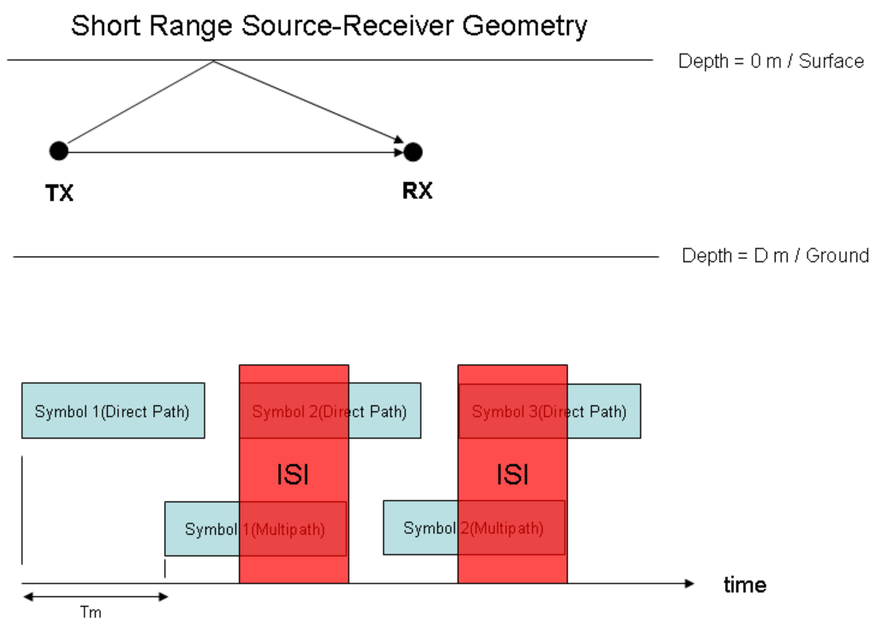

Figure 2.5: Direct-path and surface-reflected path pulse trains for a short-range source receiver geometry.

2.1.4.3 Transmission Power

Assuming that the transmitted signal p.s.d. is flat across the 3-dB bandwidth, the transmission power in watts necessary to provide a target SNR at a distance in meters from the source is determined as

$$P(l) = SNR_0 B_{3dB}(l) \frac{\int_{B_{3dB}(l)} N(f)df}{\int_{B_{3dB}(l)} A^{-1}(l,f)df} \tag{2.9}$$

We note that this is not the optimal way to shape the spectrum of the transmitted signal; however, it is often used in practice and quite sufficient for the purpose of illustrating the networking concepts.

Chapter 3

ORTHOGONAL FREQUENCY DIVISION MULTIPLEXING

3.1 General Principles

Orthogonal frequency division multiplexing (OFDM) is considered for the next generation acoustic modems as a low-complexity alternative to single-carrier modulation. Because of its simplicity, OFDM has found application in many wireless radio communications. Its application to underwater acoustic systems has been addressed recently.

3.1.1 The Concept of Multicarrier Transmission

The simple idea of multicarrier transmission is to split a data stream into K substreams of lower data rate and to transmit these data substreams on adjacent subcarriers. This can be regarded as a transmission parallel in the frequency domain, and it does not affect the total bandwidth that is needed. Each subcarrier has a bandwidth B/K, while the symbol duration T_s is increased by a factor of K, which allows for a K times higher data rate for a given delay spread.

3.1.2 OFDM as multicarrier transmission

OFDM is a spectrally efficient version of multicarrier modulation, where the subcarriers are selected such that they are all orthogonal to one another over the symbol duration, thereby avoiding the need to have non-overlapping subcarrier channels to eliminate intercarrier interference. Choosing the first subcarrier to have a frequency such that it has an integer number of cycles in a symbol period, and setting the spacing between adjacent subcarriers (subcarrier bandwidth) to be B/K, where B is the nominal bandwidth (equal to data rate), and K is the number of subcarriers, ensures that all tones are orthogonal to one another over the symbol period. Each subcarrier is modulated with a conventional modulation scheme (such as Quadrature Amplitude Modulation -QAM- or Phase Shift Keying -PSK-) at a low symbol rate, maintaining total data rates similar to conventional single-carrier modulation schemes in the same bandwidth.

One of the main reasons of using the OFDM scheme is its ability to adapt to severe channel conditions without using a complex equalizer. If the number of subcarriers, K is selected large enough, the bandwidth of each sub-carrier becomes smaller than the coherence bandwidth of the channel. In this case, the channel characteristic of each subcarrier exhibits approximately at fading and therefore the distortions on the channel can be compensated by a one-tap equalizer. Besides, the OFDM scheme is also robust against fading caused by the multipath propagation. Whereas a deep fade may cause a failure in a single carrier system, only a small part of the subcarriers in an OFDM system is destroyed by the fading and lost information on the destroyed sub-carriers can be recovered by using forward error correction (FEC) codes [20] .

In a conventional multicarrier system, the frequency band is divided into non-overlapping adjacent subbands where adjacent subcarriers are separated by more than the two sided bandwidth of each. This technique eliminates the intercarrier interference (ICI) by avoiding the spectral overlaps, but it causes inefficiency in the use of available frequency band. The OFDM scheme overcomes this inefficiency by selecting the sub-carrier frequencies as mathematically orthogonal to each other. The word "orthogonal" means that the frequency of each sub-carrier is an integer multiple of 1/T, where T is the symbol duration [22]. By this way, as shown in Fig. 3.1, the frequency band is used 50% more efficiently than a conventional system without causing an ICI. [20]

A disadvantage that results from the use of orthogonality is the need for highly accurate frequency synchronization between the transmitter and the receiver. The frequency deviation that OFDM systems can tolerate is very small as the subcarriers will no longer be orthogonal, causing ICI, or cross-talk between subcarriers.

Frequency offsets are typically caused by Doppler shifts due to motion, or mismatched transmitter and receiver oscillators. While Doppler shift alone may be compensated for by the receiver, the situation is worsened when combined with multipath, as reflections will

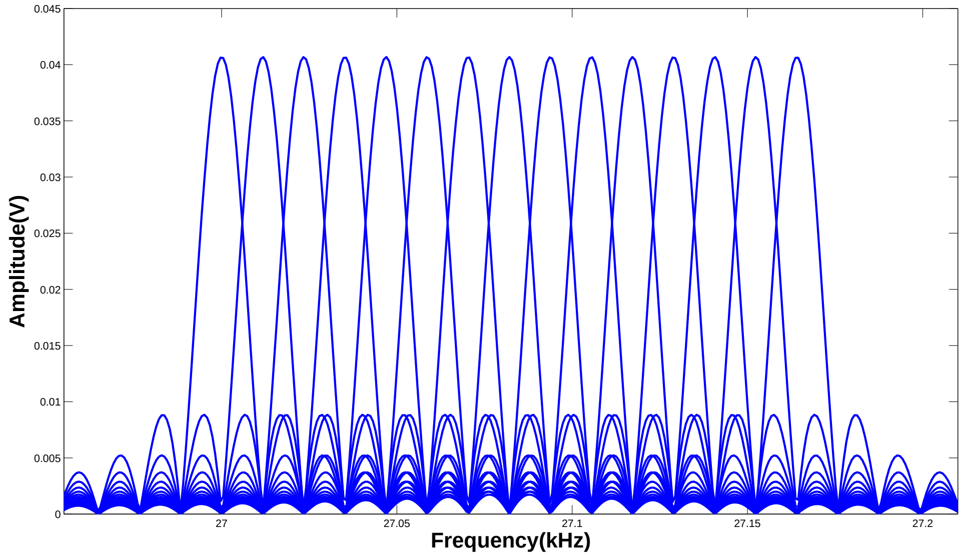

Figure 3.1: Orthogonal overlapping spectral shapes for OFDM.

appear at various frequency offsets, which is much harder to correct.
In order to completely eliminate ISI, guard intervals are used between OFDM symbols. By making the guard interval larger than the expected multipath delay spread, ISI can be completely eliminated. Adding a guard interval, however, implies power waste and a decrease in bandwidth efficiency. The amount of power wasted depends on how large a fraction of the OFDM symbol duration the guard time is. Therefore, the larger the symbol period-for a given data rate, this means more subcarriers-the smaller the loss of power and bandwidth efficiency.

3.1.3 Modulation using FFT

Due to the orthogonality of OFDM subcarriers, the modulator and demodulator can be efficiently implemented using the FFT algorithm on the receiver side, and the inverse FFT, or IFFT, on the transmitter side. As it has been claimed, on the transmitter side the IFFT of a signal $X(k)$, where k denotes the frequency component index, is

$$x(l) = \frac{1}{K}\sum_{k=0}^{K-1} X(k)e^{j2\pi kl/K} \qquad \text{l=0,....,K-1} \tag{3.1}$$

where K designates the number of frequency components, and $x(l)$ is the resulting sampled signal, which is formed by the sum of the modulated frequency components $X(k)$. To retrieve again the digital frequency components, the inverse equation must be used which corresponds to the K-point FFT of $X(k)$.

3.1.4 Advantages and Disadvantages of OFDM

The main advantage of the OFDM modulation scheme in terms of practical implementation is that it enables channel equalization in the frequency domain, thus eliminating the need for potentially complex time-domain equalizers. The following advantages of OFDM should be mentioned:

- Simple and effective channel equalization in the frequency domain
- High spectral effciency
- Low sensitivity to time synchronization errors
- Robustness against Inter-Channel Interference (ICI)
- Robustness against Inter-Symbol Interference (ISI) and fading caused by the multipath channel
- Efficient implementation using the FFT, avoiding the need for complex subchannel flters

The major disadvantages of OFDM are:

- Sensitivity to frequency offsets
- High Peak to Average Ratio (PAR), with a subsequent difficulty to optimize the transmission power

Chapter 4

TRANSMITTER DESIGN

4.1 Transmitter Design

In this section, system model of transmitter and the packet structure of transmitted signal are explained.

In our Transmitter design, we prefer a zero-padded (ZP)-OFDM system instead of cyclic prefix (CP). The main reason behind that CP can be spend too much transmission power and it is not so effective in underwater channels where long delay spread occurs[16].

As we use ZP-OFDM we will have guard interval after each OFDM block. Let T_g denotes duration of this guard interval while T denotes the duration of one OFDM block. As a result, the total OFDM block duration becomes $T_t = T + T_g$ where the frequency spacing is $\Delta f = 1/T$.

Based on frequency spacing, kth subcarrier frequency of one ZP-OFDM block will be;

$$f_k = f_{low} + k \cdot (\Delta f), k = 0, ..., K-1 \tag{4.1}$$

where f_{low} denotes the lowest subcarrier frequency. So one ZP-OFDM block will have a bandwidth of $B = K \cdot \Delta f$.

Each subcarrier will be accommodated by a data symbol, so there will be K data or pilot symbols in one ZP-OFDM block. In some cases, based on design decisions, null subcarriers may also occur in OFDM blocks. In this case there will be K_d data or pilot symbols and K_n null subcarriers. Data symbols are denoted as $s[k]$, which means data symbol at kth subcarrier. The transmitted signal at passband of one ZP-OFDM block is given by;

$$s(t) = Re\left\{\left[\sum_{k=0}^{K-1} s(k) e^{j2\Pi k \Delta f t} g(t)\right] e^{j2\Pi f_{low} t}\right\}, t\epsilon[0, T+T_g] \tag{4.2}$$

where $g(t)$ is rectangular pulse shape with duration of T and unit amplitude that defines the zero-padding operation.
With the N_d of that ZP-OFDM block and a synchronization preamble, a packet is generated. The structure of a packet is shown in Fig. 4.1.

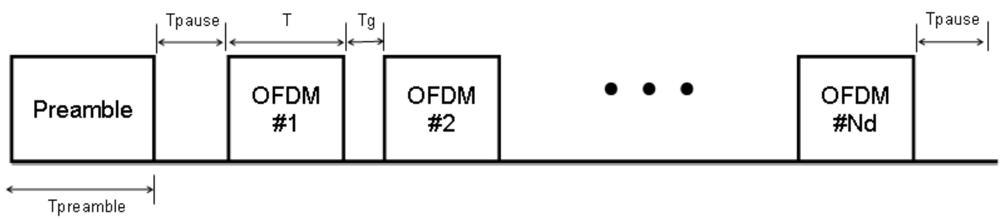

Figure 4.1: Packet Structure

For building up such a packet structure, a transmitter design is used whose system model is shown in Fig. 4.2.
As it is shown in Fig. 4.2, the system starts with a 'Mapping' block. In this block, information bits are mapped into symbols by using Quadrature Phase Shift Keying (QPSK) modulation scheme. In the second block which is shown as 'S/P', the information symbols generated are serial-to-paralel converted into K streams for next block.
In next block, IFFT modulation operation is made. This block is explained in Section 3.1.3. In addition, an upsampling operation is made for correct demodulation of OFDM blocks. Based on Nyquist Sampling theorem, sampling frequency f_s should meet the requirement that $f_s > 2 \cdot f_{high}$ where f_{high} denotes the highest contained transmitted signal. Otherwise, aliasing will occur and our signal will be distorted severely. In our system, the f_s is selected as and integer multiple of transmitted signal bandwidth of 12 kHz which is denoted by B. This idea simplifies the upsampling operations at transmitter and downsampling operations at receiver for baseband signal processing [7]. We use a center frequency f_c of 27 kHz based on our system properties which is detailed in Section 6.1.2. As a result, with a B of 27 kHz, we have $f_{high} = 33$ kHz.

Considering all these factors, we chose our f_s as 96 kHz which is an integer multiple of

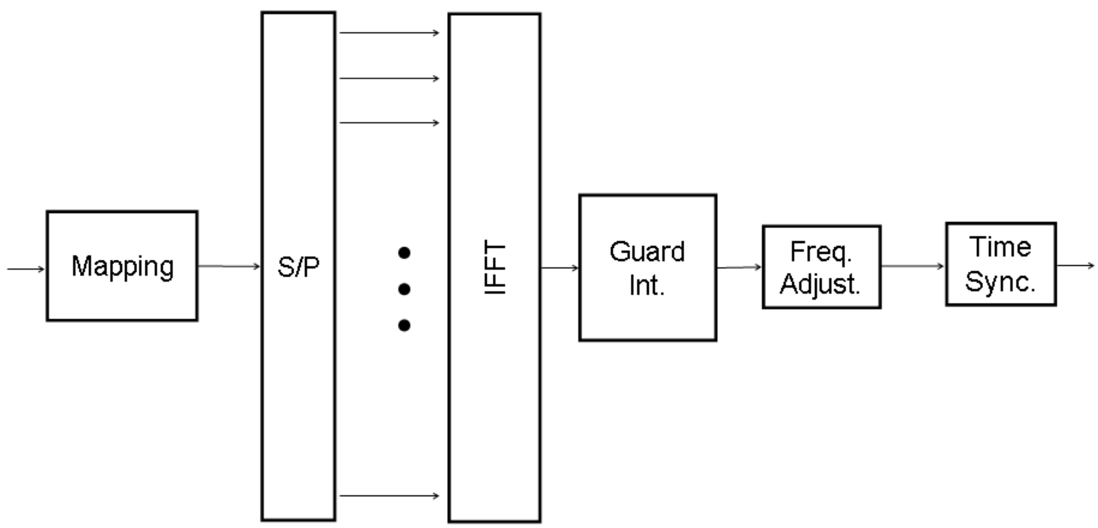

Figure 4.2: Transmitter System Model

B and fulfills the Nyquist sampling theorem, but the most important our system could work properly at it. For reaching f_s rate, $7 \cdot K$ zeros have been appended to K subcarrier symbols. For better understanding, transmitted signal model in the frequency domain is shown in Fig. 4.3.

After then N_u-point IFFT was performed as in the following equation.

$$u(l) = \sum_{k=0}^{N_u-1} \check{s}(k) e^{j2\Pi kl/N_u}, l = 0, 1, ..., N_u - 1 \tag{4.3}$$

where N_u is the number samples during time T, $\check{s}$ is the vector of samples whose first K positions are accommodated by subcarrier symbols while the other $7K$ spots contain appended zeros. As a result, a baseband signal at a rate of f_s is generated.

After a baseband signal generated, a guard interval is inserted after each OFDM block which has a duration of T_g for forming the ZP-OFDM structure. After then, the frequency adjustment is done, and signal became a passband signal which is shown in Eq.4.2 where

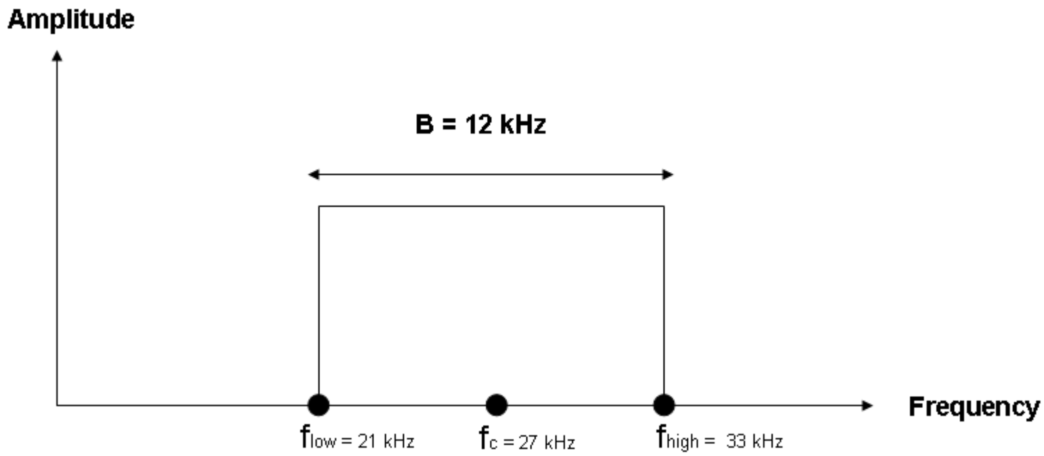

Figure 4.3: Transmitted Signal Model

$f_c = 27$ kHz and $B = 12$ kHz so f_{low} is around 21 kHz.

In the last block of the transmitter, time synchronization preamble is inserted at beginning of each packet structure as it is shown in Fig.4.1. The time synchronization is vital for locating the OFDM blocks for demodulation. Its duty is to provide correct timing for the system to receive data correctly and avoid any inter-block interference (IBI). In our system, timing synchronization preamble is a pseudo-random PN sequence of length 127 and it is quadrature-modulated using the center frequency f_c of 27 kHz. It is duration is 100 ms. The time synchronization preamble is transmitted with the highest power for maximizing the probability of detection. As another property, a good designed preamble must have good correlation properties that only a main peak has to occur as a result of autocorrelation operation.

There is a pause time of 50 ms after preamble, right before the beginning of the OFDM blocks. There is also another pause time of 50 ms that ends the packet. These two pause intervals, complete the packet structure shown in Fig. 4.1 and transmitted signal is occurred which is shown in Fig. 4.4.

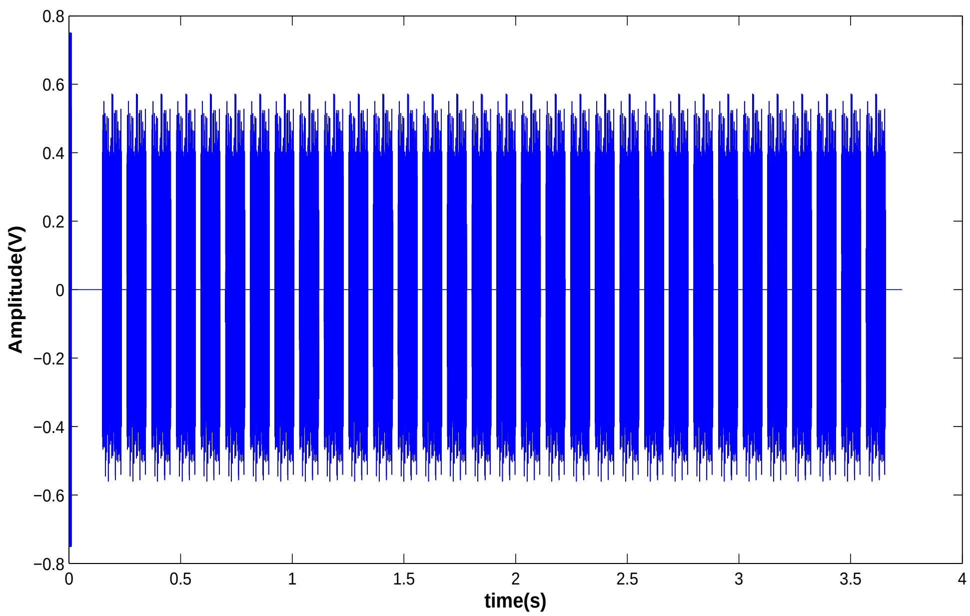

Figure 4.4: Transmitted Signal

Chapter 5

RECEIVER DESIGN

In this section, system model of receiver and receiver algorithms are explained.

5.1 System Model

The OFDM receiver model is designed based on the transmitted signal and considering underwater acoustic channel effects. Receiver system model is shown in Fig. 5.1 where BPF and LPF stands for band-pass filtering and low-pass filtering respectively.

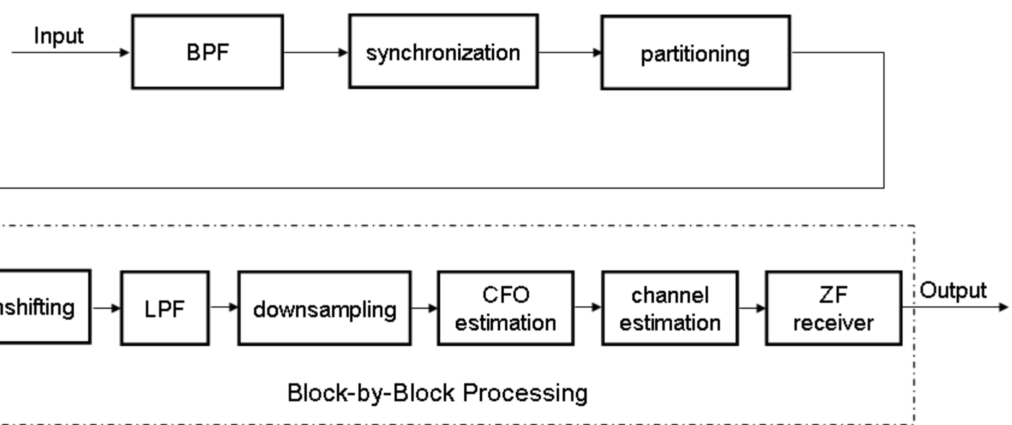

Figure 5.1: Receiver System Model

Once the signal is received from the channel, it is directly sampled with hardware in the system and all processing is done in discrete-time signals. After received signal is converted into discrete-time, band-pass filtering is performed in order to minimize out band noise on the received signal.

After filtering is performed, time synchronization operation is done for correct reception of the OFDM blocks. For time synchronization, cross-correlation of received signal and known preamble is used, details are given in Section 4.1. The cross-correlation is performed for a length of N_{sync} , that is the number of samples between the beginning of preamble and first OFDM block which contains pause time after preamble. As a result of cross-correlation operation, a high peak occurs where preamble is detected in received signal based on the properties of preamble.

When time synchronization is done, received packet is partitioned into OFDM blocks and after that operation all processing is done block-by-block.

In the beginning of the block-by-block processing, OFDM block are downshifted in frequency and a low-pass filtering is performed. In this step, signal is downsampled to a sampling frequency of 12 kHz for applying the the receiver algorithms. After then, carrier-frequency-offset (CFO) estimation and compensation is performed. After CFO estimation, overlap-add (OLA) based demodulation for OFDM [16] is carried out. This operation converts linear modulation to circular convolution and then converts data to frequency-based for demodulation. In the following step, channel estimation operation is carried out and linear zero-forcing(ZF) receiver is used for determining the received symbols.

5.2 Algorithms

In this subsection, algorithms that has been used in System Model are explained. The proposed algorithms are taken from [8, 15].

5.2.1 Pilot Tone based Channel Estimation

The receiver needs channel frequency response before processing an equalization operation. In that manner, pilot tone based channel estimation is applied. In this method, K_p symbols of K symbols are chosen as known pilot symbols and used in channel estimation process. In selecting K_p pilot symbols proposed rules in [15] are followed for minimizing the complexity. This rules are;

- **r1)** K_p pilot symbols are chosen equally spaced at subcarriers.

$$0, M, 2M, ..., (K_p - 1)M, M = K/K_p \tag{5.1}$$

  where subcarrier indices are denoted by $p_1, p_2, ..., p_{K_p}$.

- **r2)** Pilot symbols are PSK signals that have unit amplitudes.

The received signal in kth subchannel after CFO estimation can be shown as,

$$z[k] = H(k)s[k] + v(k) \tag{5.2}$$

where $v(k)$ is additive noise and $H(k)$ is the channel's frequency response on the kth subchannel;

$$H(k) = \sum_{l=0}^{L} h(l)e^{-j2\Pi kl/K}, k = 0, ..., K-1 \tag{5.3}$$

If $K_p > L + 1$, then channel taps can be computed by least squares (LS) formulation as it is shown in Eq. 5.4 (where L denotes channel taps.)

$$z_p = D_s V h + v \tag{5.4}$$

where

$$D_s = \begin{bmatrix} s[p_1] & & & \\ & . & & \\ & & . & \\ & & & . & \\ & & & & s[p_{K_p}] \end{bmatrix} \quad V = \begin{bmatrix} 1 & e^{-j2\Pi p_1/K} & . & . & . & e^{-j2\Pi p_1 L/K} \\ . & . & . & & & . \\ . & . & & . & & . \\ . & . & & & . & . \\ 1 & e^{-j2\Pi p_{K_p}/K} & . & . & . & e^{-j2\Pi p_{K_p} L/K} \end{bmatrix}$$

$$h = \begin{bmatrix} h_o \\ . \\ . \\ . \\ h_L \end{bmatrix} \quad v = \begin{bmatrix} v_{p_1} \\ . \\ . \\ . \\ v_{p_{K_p}} \end{bmatrix} \quad z_p = \begin{bmatrix} z_{p_1} \\ . \\ . \\ . \\ z_{p_{K_p}} \end{bmatrix}$$

As pilot symbols are equispaced, $V^H V = K_p I_{L+1}$ [23] and as they have unit amplitude, $D_s^H D_s = I_{K_p}$ where $(.)^H$ denotes Hermitian transpose. Based on these properties, LS formulation in 5.4 could be written as;

$$\hat{h}_{LS} = \frac{1}{K_p} V^H D_s^H z_p \tag{5.5}$$

As time-domain channel estimation is made by using 5.5, we could reach frequency domain channel estimation by using 5.3. As a result of that operation, a LS fitting error is occurred and it can be calculated as;

$$\epsilon_{LS} = \|z_p\|^2 - K_p^{-1} \left\| V^H D_s^H z_p \right\|^2 \tag{5.6}$$

5.2.2 CFO Estimation

Carrier-frequency-offset estimation and compensation is a vital algorithm process for OFDM in a UWA channel. If this compensation is not applied then, inter-subcarrier-interference (ICI) severely affects the channel estimation and receiver performances. This ICI is caused by the lost of orthogonality among subcarriers in OFDM blocks which is due to fast variation of UWA channel. In our system we use two different CFO estimation methods which are detailed in Section 5.2.2.1 and Section 5.2.2.2. As a note, CFO estimation can change from block to block and it is denoted by ϵ.

5.2.2.1 CFO Estimation Method I

In this method, CFO estimation technique in [8] is used , where the CFO estimation is performed based on the LS fitting error in 5.6.

First of all, a matrix is defined for CFO compensation;

$$\Gamma(\epsilon) = diag(1, e^{j2\Pi T_s \epsilon}, ..., e^{j2\Pi T_s \epsilon (K+L_{zp}-1))}) \tag{5.7}$$

where L_zp denotes number samples(at $f_s = B$) in a guard interval, which is explained in section 4.1 and T_s stands for sampling interval that equals to T/K.

After CFO compensation matrix is defined, an equation is made up for CFO compensation and creating input data for pilot-tone based channel estimation. This equation is;

$$z(\epsilon) = FFT_K(R_{ola}\Gamma(\epsilon)^{-1}y) \tag{5.8}$$

where FFT_K, y , $z(\epsilon)$, R_{ola} denote K-point Fast-Fourier Transform, processed signal, created input data for pilot-tone channel estimation and matrix of overlap-adding operation respectively. The R_{ola} is a $KxK+L_{ZP}$ matrix which is equal to $[I_K, I_{ZP}]$ where I_M denotes a MxM identity matrix. R_{ola} in our system defines an operation of adding last L_{ZP} entries of y to first L_{ZP} of them while holding the first K entries.

As we create a $z(\epsilon)$, we could use LS fitting error with one dimensional search for finding best value for ϵ. As a result, we reached a CFO estimator model as it is shown in 5.9.

$$\hat{\epsilon} = argmin_{\epsilon}\left\{\|z_p(\epsilon)\|^2 - K_p^{-1}\left\|V^H D_s^H z_p(\epsilon)\right\|^2\right\} \tag{5.9}$$

5.2.2.2 CFO Estimation Method II

In this method, the CFO estimation technique in [15] is used, where the CFO estimation is performed based on the null subcarriers. As it is mentioned in Section 4.1, using null subcarriers is a design decision. After this decision has been made, the number of null subcarriers and their positions should be decided. In our system, the proposed design in [24] for null subcarriers is used. There are $K_n = 56$ null subcarriers, half of them are allocated at the edges of the frequency bands while the other half are randomly placed at available spots. The null subcarrier indices are denoted by $n_1, n_2, ..., n_{K_n}$. As null subcarrier properties are chosen then CFO estimator can be designed.

First of all, a cost function is defined which shows the total energy on null subcarriers;

$$J(\epsilon) = \sum_{k=n_1}^{n_{K_n}} \left|f_k^H \Gamma^H(\epsilon) y\right|^2 \tag{5.10}$$

where $f_k = [1, e^{\frac{j2\Pi k}{K}}, ..., e^{\frac{j2\Pi k(K+L-1)}{K}}]^T$ and $(.)^T$ denotes transpose.

The total energy on null subcarriers determines the ICI scatters that comes from the neighboring subcarriers which should be minimized for better demodulation performance. Therefore, a one dimensional search is proposed which is similar the MUSIC-like algorithm for CP-OFDM in [25] for finding the lowest cost function and this will be the CFO estimator in the system. The CFO estimator is:

$$\hat{\epsilon} = argmin_{\epsilon} J(\epsilon) \tag{5.11}$$

As we estimate CFO, we use CFO compensation (5.8) and reach input data for pilot-tone channel estimation.

5.2.3 Zero-Forcing Receiver

Linear zero-forcing (ZF) receiver which is found by R.Lucky [26], is used like it is proposed in [8, 15, 24]. As channel transfer function in frequency domain is found by (5.3), we can find receive transmitted symbols. The receiver is defined as;

$$\hat{s}(k) = (H^H(k)H(k))^{-1}H^H(k)z(k) \tag{5.12}$$

where z and $\hat{s}$ denotes the data came from CFO estimation and received symbols respectively.

Chapter 6

SYSTEM DEPLOYMENT

In this chapter, hardware properties of receiver and transmitter are explained.

6.1 Underwater Experiments

Once the simulations are finished successfully, system tests are performed in the underwater channel. Moreover, the limits in terms of data rate and useful bandwidth are reached to achieve an optimal performance with the selected hardware.

6.1.1 Deployment

The underwater tests are performed at Bilkent Lake Facility, Ankara. The transmitter was submerged at a depth of about 5 meters. The receiver was submerged at a depth of about 5 meters.
The experimental setup and depth profile of Bilkent Lake Facility are shown in Fig. 6.1.
In Fig. 6.2, the photo of Bilkent Lake Facility is shown.
The illustrative block diagram for the underwater tests is shown in Fig. 6.3 for the transmitter (left), and for the receiver(right)

6.1.2 Hardware

- Laptop

  The transmitting side laptop is used to generate data with MATLAB. MATLAB's Data Acquisition Toolbox is used to transmit the data to the NI USB-6251 BNC DAQ Card and from it to the transmitting hardware, which in this case is the Krohn-Hite Model 7500 Power Amplifier coupled with the transducer by an impedance matching

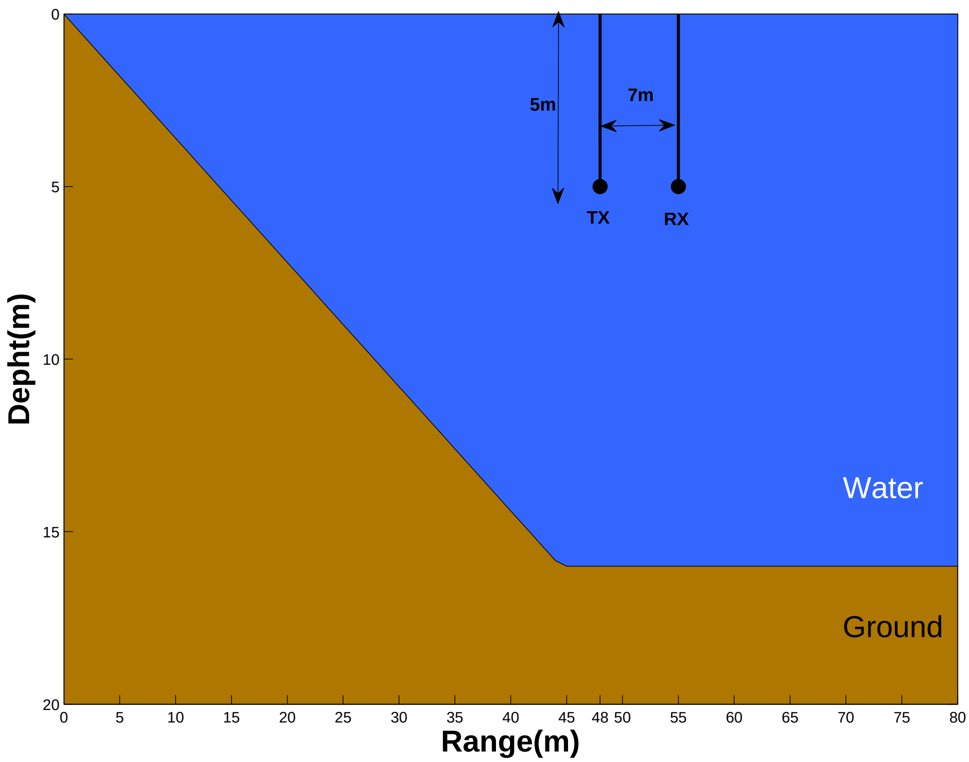

Figure 6.1: Experimental Setup

transformer. On the receiving side, the laptop receives the data from the USB-6251 BNC DAQ Card via a C++ script and the demodulation is performed.

- **National Instruments USB-6251 BNC Data Acquisition(DAQ) Card**

  NI USB-6251 BNC Data Acquisition(DAQ) Card is used as an interface that allows the transmission of the generated acoustic signals by sampling the analog signal at the desired rate(upto 1 Mbps) provided by the laptop computer.

- **Krohn-Hite Model 7500 Power Amplifier**

  The signal transmitted by the NI USB-6251 BNC DAQ Card is further amplified by the Krohn-Hite Model 7500 Power Amplifier, to adjust the signal power to the transmission requirements in the underwater channel. The power response of the Krohn-Hite Model 7500 Power Amplifier, is shown in Fig. 6.4.

- **Impedance matching circuitry**

Figure 6.2: Bilkent Lake Facility

Prior to sending the signal to the transducer, an impedance matching transformer adjusts the signal for maximum power transmission to the transducer.

- **Custom Transducer**

  The transducer is omni-directional. It has a Transmitting Voltage Response (TVR) of 130 dB at its resonance frequency which is 30 kHz. The TVR decays at lower and higher frequencies, thus limiting the transmission bandwidth to about 12 kHz.

- **Reson TC400 Hydrophone**

  Reson TC400 ideal standard reference hydrophone has been chosen for the reception of the acoustic OFDM signal. Its most important characteristic is the wide frequency range and the relatively high transmitting sensitivity. The horizontal directivity pattern and receiving sensitivity is provided in Fig. 6.5 .

- **Reson VP2000 Preamplifier**

  Once the signal is picked up by the hydrophone, the Reson VP2000 preamplifer

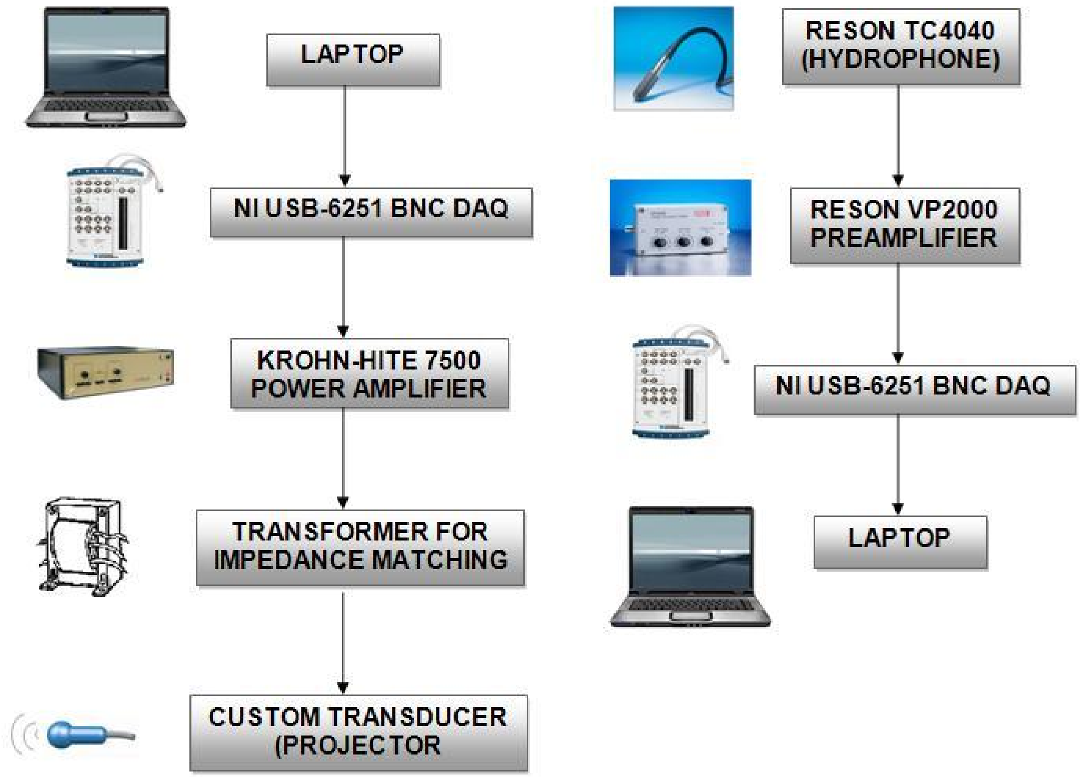

Figure 6.3: Transmission block diagram for underwater tests, transmitter(left) and receiver(right)

amplifies and filters the received signal. The characteristics of the high-pass and low-pass filters are given in Fig.6.6. As it can be seen, the filter response is adjustable depending on the signal frequency components.

- **National Instruments USB-6251 BNC Data Acquisition(DAQ) Card** NI USB-6251 BNC Data Acquisition(DAQ) Card is also used as an interface that allows the reception of the generated acoustic signals by sampling the analog signal at the desired rate(upto 1 Mbps) provided by the Reson VP2000 preamplifier, and transmitting it to the receiving laptop.

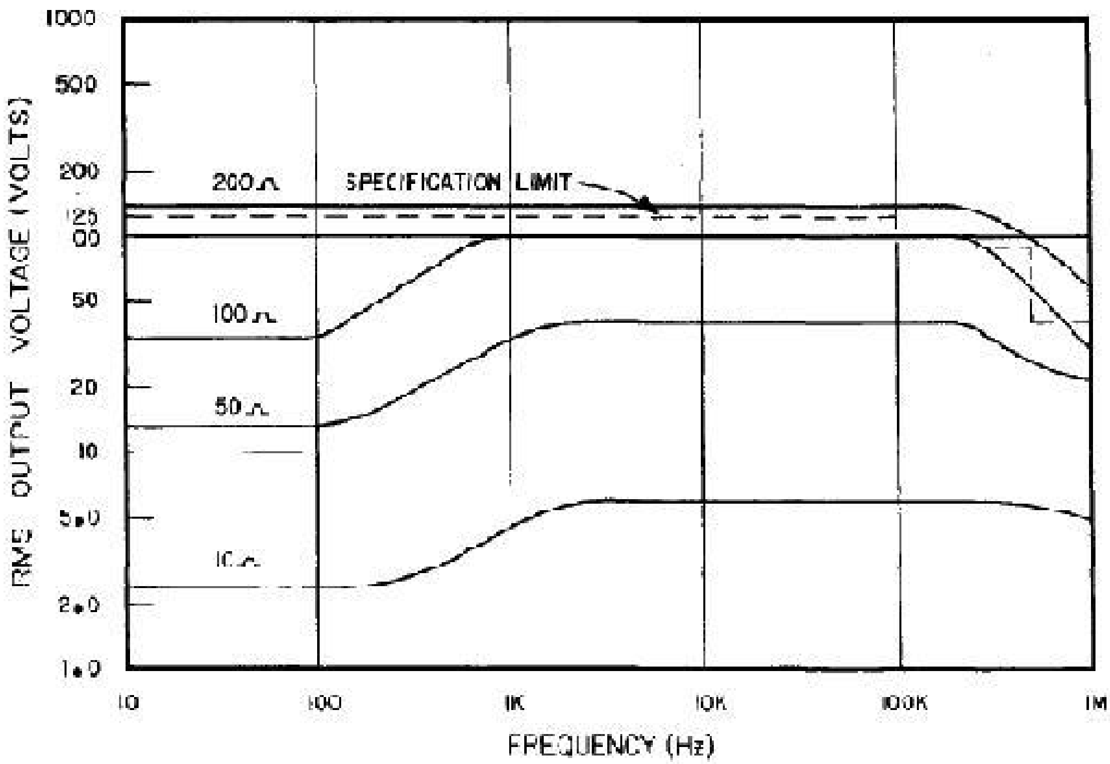

Figure 6.4: Power response of the Krohn-Hite Model 7500 Power Amplifier

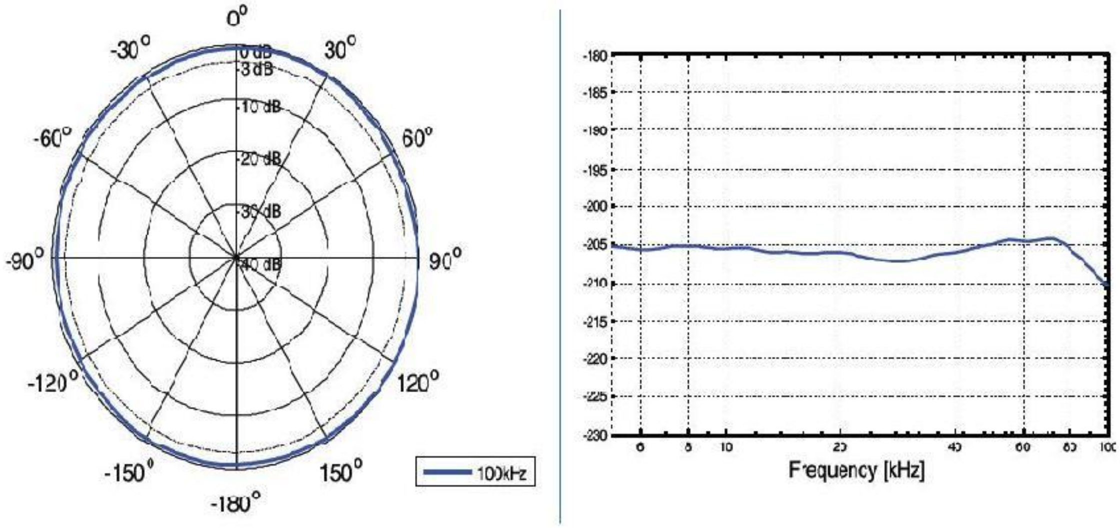

Figure 6.5: Horizontal directivity pattern (left) and receiving sensitivity (right) of the Reson TC4040 hydrophone

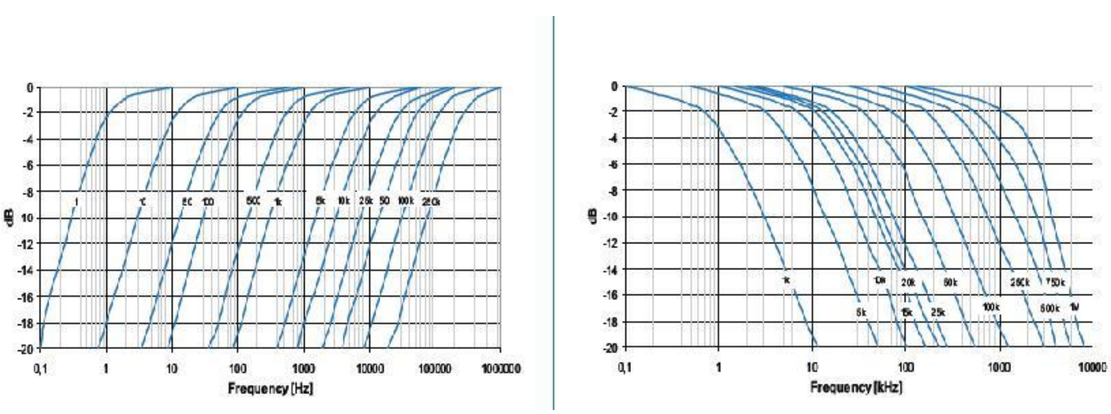

Figure 6.6: High-pass filter (left) and low-pass filter (right) frequency responses of the Reson VP2000 Preamplifier

Chapter 7

EXPERIMENTAL RESULTS

Experiments are performed to test the performance of the selected algorithms along with the deployed system. In this section the results are analyzed. Also some comparisons are made between our system performance and some other systems in the literature.

Two tests were done at Bilkent Lake Facility, by using the system deployment which is mentioned at the System Deployment section. The second test had the same system configuration except that transmitted signal contained null subcarriers.

7.1 Underwater Experiment I

The bandwidth of the OFDM signal is $B = 12$ kHz, and the carrier frequency is $fc = 27$ kHz. The transmitted signal thus occupies the frequency band between 21 kHz and 33 kHz. We use zero-padded OFDM with a guard interval of $Tg = 25$ ms per OFDM block. The number of subcarriers used in the experiment is $K = 1024$. The number of pilot subcarriers is $K_p = 256$ which is equal to $K/4$. The subcarrier spacing is $\Delta f = 11.72$ Hz and the OFDM block duration is $T = 1/\Delta f = 85.33$ ms. QPSK modulation is used. For $K = 1024$ each packet contains $N_d = 32$ OFDM blocks, respectively. The total number of information symbols per packet is 32768.

The system deployment is shown in Fig. 6.1. By this system deployment and the hardware (see Section 6.1.2), the received signal was directly A/D converted. The received signal is shown in 7.1.

After signal is received and analog to digital converted, it is processed based on the receiver processing shown in Fig. 5.1. In the following subsections, the numerical results for this processing operation are explained.

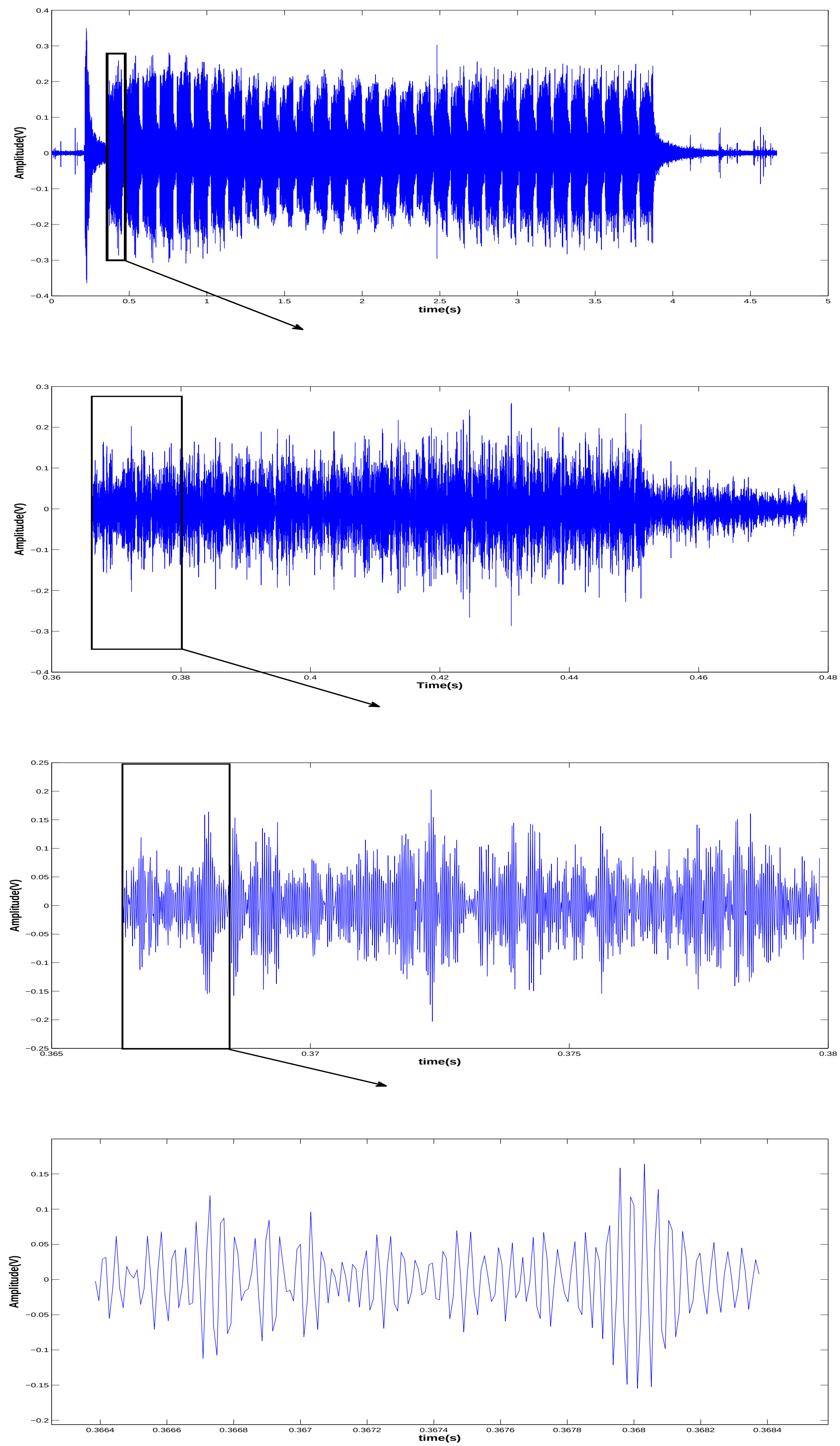

Figure 7.1: Received Signal

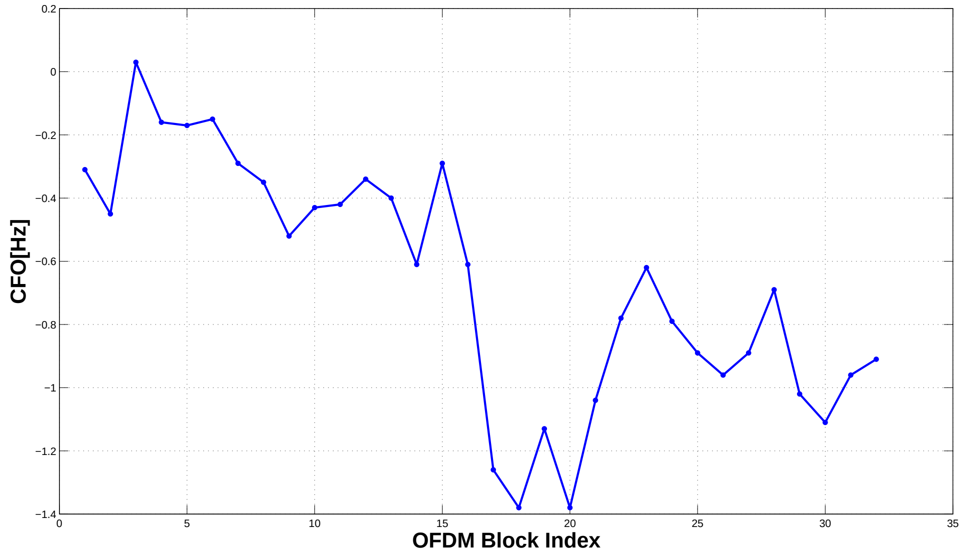

Figure 7.2: CFO Estimation

7.1.1 CFO Estimation

CFO estimation was performed on each 32 block in the data separately, as detailed in Section 5.2.2.1. In Fig. 7.2, the CFO estimation for each OFDM block is shown. We observe that estimated CFO for each block does not change much but we cannot accept it as constant for each block. Otherwise, the receiver performance could be severely effected by(ICI).

We observe that CFO estimates vary between 0 and -1.4 Hz. These CFO estimates can be treated as Doppler shift and as our system works at a center frequency of 27 kHZ, they can be translated into moving speeds that vary between 0 and 0.078 m/s (or 0 and 0.151 knots).

7.1.2 Channel Estimation

Channel Estimation was performed based on $K_p = K/4$ equispaced pilot-tones, as detailed in Section 5.2.1. In Fig. 7.3, channel estimations for 32 blocks are shown.

We observe that each OFDM block have similar channel estimates. As we use stable deployment positions for our system, we except that similarity. So we can observe channel estimation of one block to understand the channel characteristics.

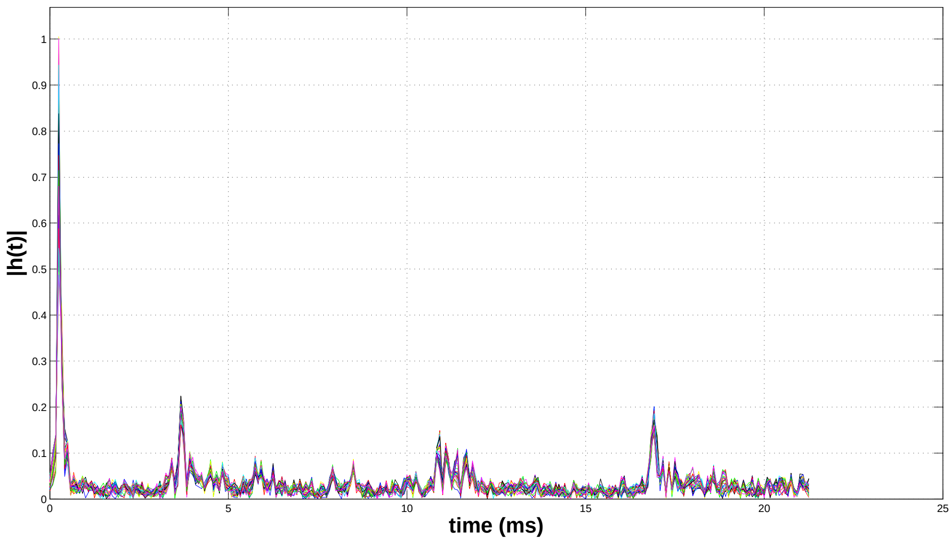

Figure 7.3: Channel Estimation for all blocks

From Fig. 7.4, we observe that there is a strong direct path between transmitter and receiver. Also, three more paths are observed which are weaker than direct path. Following assumptions could be made about those three paths:

- First of all, we assume that first path after direct path is from the surface bounce. This assumption is supported by our computation using channel geometry.

  From Section 6.1.1, we know that the direct path distance is 7 m and both receiver and the transmitter at a depth of 5 m. So, the delay between the surface bounce and the direct path is

  $\left(2 \times \sqrt{(3.5)^2 + 5^2} - 7\right)/1500 = 3.47ms$

- Secondly, we assume that second path after direct path is from the bottom bounce. The depth of the bottom is roughly 11 m from both receiver and transmitter.

  $\left(2 \times \sqrt{(3.5)^2 + 11^2} - 7\right)/1500 = 10.73ms$

- Lastly, we assume that third path after direct path is a summation two different paths. One of them comes from a surface bounce and then a bottom bounce while the other one comes from a bottom bounce and then a surface bounce. As receiver and transmitter depths are equal and bottom topology is uniform and flat, these two

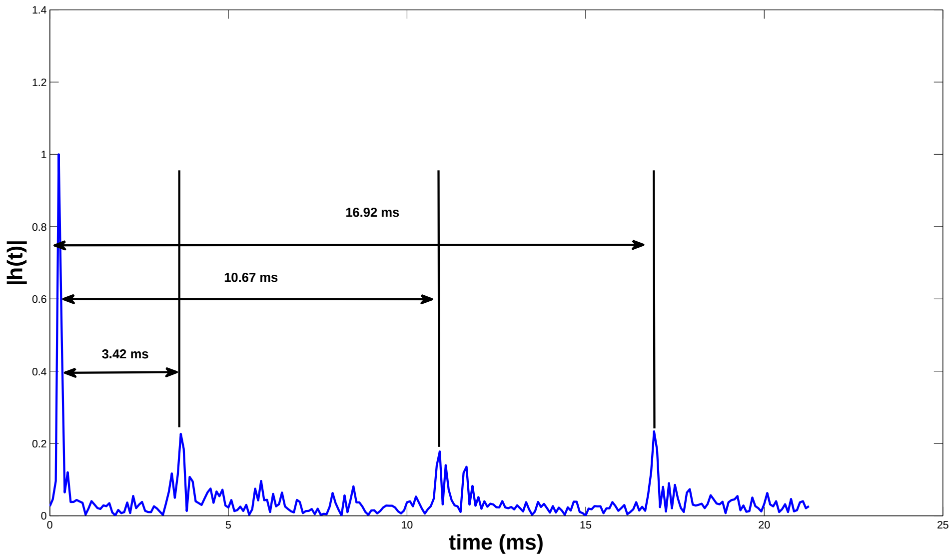

Figure 7.4: Delay Spread

paths have same distance between receiver and transmitter. So their signals sum up and create the third path after the direct path. For supporting this assumption, we compute the delay of that path. We made the computation for surface bounce, bottom bounce path.

$$\left(2 \times \sqrt{(0.887)^2 + 5^2} + 2 \times \sqrt{(2.613)^2 + 11^2} - 7\right)/1500 = 17.18ms$$

In Fig. 7.5, all paths are shown and denoted with an abbreviation and the duration of the path.

The abbreviations are explained in the Table 7.1

Table 7.1: Path Definitons

DP	Direct Path
BB	Bottom Bounce
SB	Surface Bounce
SB - BB	Surface Bounce and Bottom Bounce respectively
SB - BB	Bottom Bounce and Surface Bounce respectively

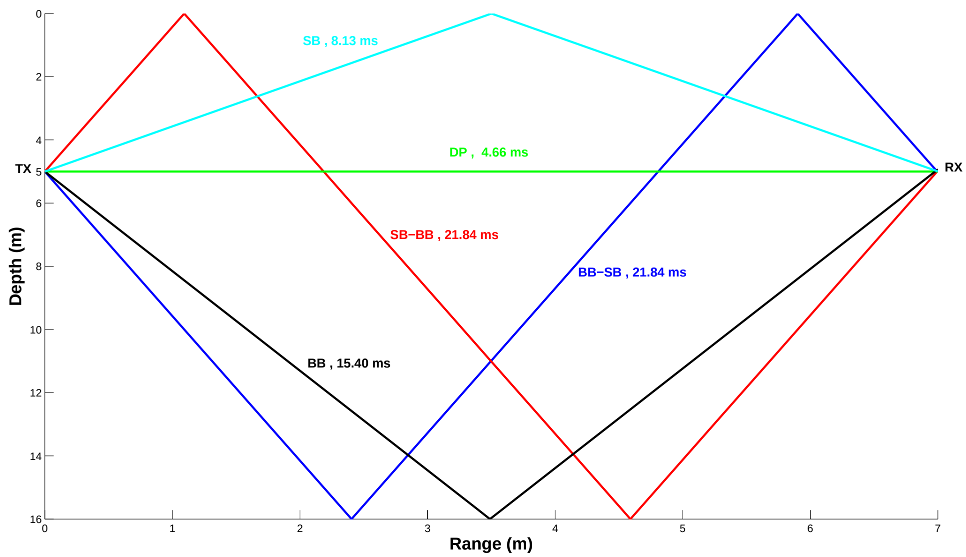

Figure 7.5: Paths of the Signal

7.1.3 BER Performance

In this part, we observe the bit error rate (BER) performance of our system.

After CFO and channel estimation, the OFDM signal is demodulated for each block separately and BER performances are determined. As it is explained in Section 5.2.3, a zero-forcing receiver is used. We observe the results of this receiver as symbols and examine our system's performance based on them. As a first result, Fig. 7.6 shows the received QPSK constellations.

As a second result, Fig. 7.7 shows the BERs of each OFDM block in a packet. We observe BER varying between 10^-1 and 10^-2. For examining our system BER performance we compare results with similar system's results in the literature. First of all we start with the system where we get the idea of our system structure. In [8] , BER varying between 10^-2 and 10^-3.

As a first intuition, we can say that this system performs better than our system, but for a fair comparison we should not ignore some points which are effective in performance results. These are; the environmental effects of place where the system tests took place, the system deployment and it's properties.

In [8], the tests took place at deep water where the receivers and transmitters were placed

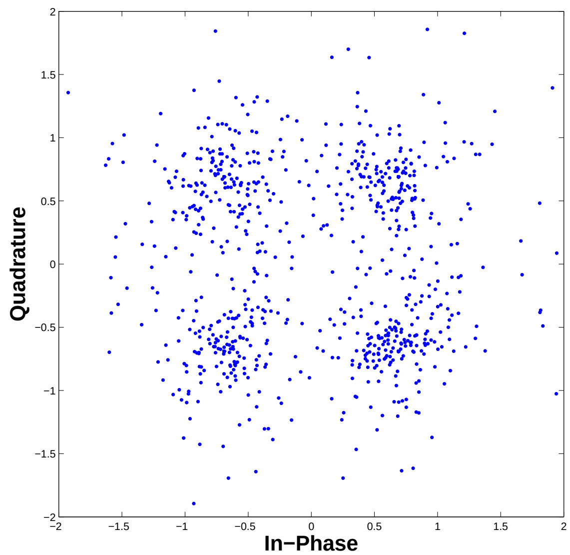

Figure 7.6: Received QPSK constellations of first OFDM block

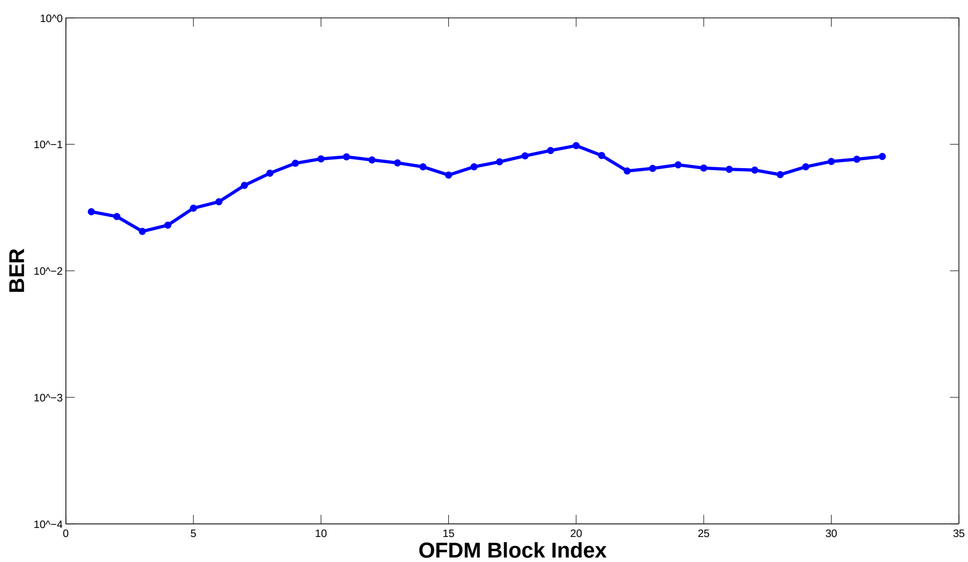

Figure 7.7: BER for each OFDM block in a packet

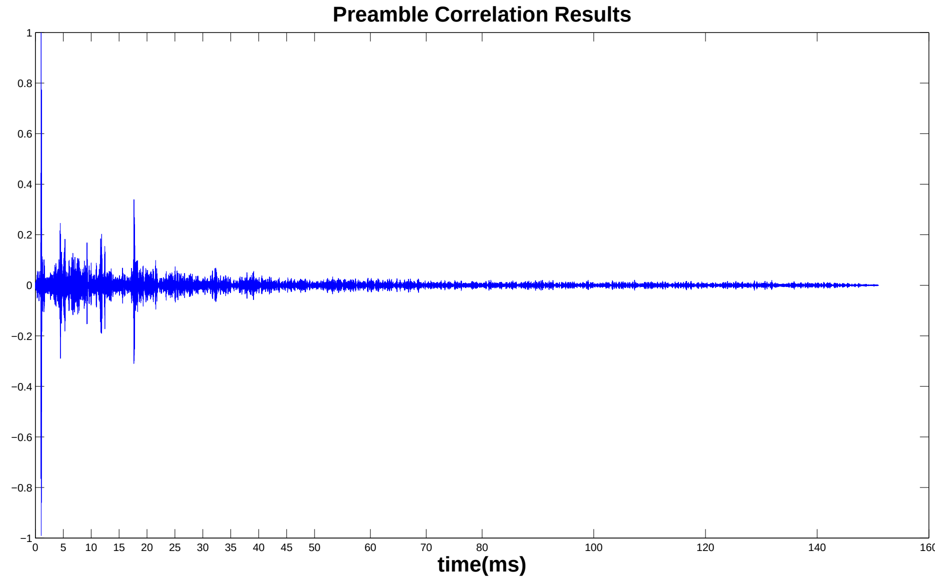

Figure 7.8: Estimated Channel response by using PN sequence matching

at a depth of 12 m. There was a transmission range of 2.5 km. When we came to the system parameters, this system has the same packet structure which is detailed in Section 4.1. The other system parameters are listed in Table 7.2.

Table 7.2: System Parameters

Signal bandwidth	$B = 24$ kHZ
Guard interval	$T_g = 25$ ms
Number of subcarriers	$K = 1024$
Number of pilot subcarriers	$K_p = K/4$

Now we know environmental and system parameters in [8], we could start to compare performance results of the systems.

In [8], based on transmitter and receivers positions, received signal has very small delay spread of 6.25 ms. When this delay spread is compared to guard time $T_g = 25ms$, as it is smaller than guard time, there was no interblock interference (IBI) in the received block.

In our system, based on transmitter and receiver positions, received signal has very large delay spread. The channel has very severe conditions because of strong multipath after the guard time of 25 ms. For observing this strong multipath effect, channel response is estimated by using PN sequence preamble matching, detailed in Section 5.1. This strong multipath effects can be observed in Fig. 7.8. Based on that figure, there are many strong paths after 25 ms. This long delay spread is caused by reflections from the shore. As our transmitter works omni-directional, signal also is sent through the shore which is shown in Fig. 6.1, and then received and creates a long delay spread. With the channel delay spread longer than the guard time of 25 ms, interblock interference (IBI) occurs.

As a result, we observe no inter-block interference (IBI) in [8] while there our system has IBI. We interpret that IBI affects BER performance significantly. This interpretation is supported by another article of the same research group [15].

In [15], similar underwater multicarrier communication is used and two different tests are conducted in different environments and their performance results are observed. In the first test, the channel delay spread is shorter than guard time while the delay spread is longer than guard time in the second one. It is mentioned that IBI is occurred when delay spread is longer than guard time. In [15], it is observed that BER is severely affected because of the IBI, so a method should be applied to reduce IBI. But as their have multiple receivers and channel coding, they trust on their receiver's robustness and did not use channel shortening approach to reduce the IBI (e.g. methods from [27, 28, 29]. By using multiple receivers with multichannel reception method and channel coding, their system reaches to reasonable BER performances.

In addition to that, we could observe the signal-to-noise ratio (SNR) to understand the severe IBI effect on the receiver. When the SNR is observed where there is no IBI, it is around 30 dB. On the other hand, when SNR is observed in the presence of IBI, then it became signal-to-noise and distortion ration(SINAD) of 10 dB. The reason behind that we considered all multipath effect after the guard interval as additive noise like in the [15]. Therefore, the SINAD value decreases as multipath spread is longer than guard interval. As SINAD decreases, BER rate increases. As a result, we observed severe IBI effect on BER performance by using SINAD values.

Based on results and explanations reached in [15], we could say that our systems BER is worse than system BER performance in [8] because of the long channel delay spread based on receiver and transmitter deployment and environmental properties. If our system test were conducted at the same environment with environment in [8], system BER will be

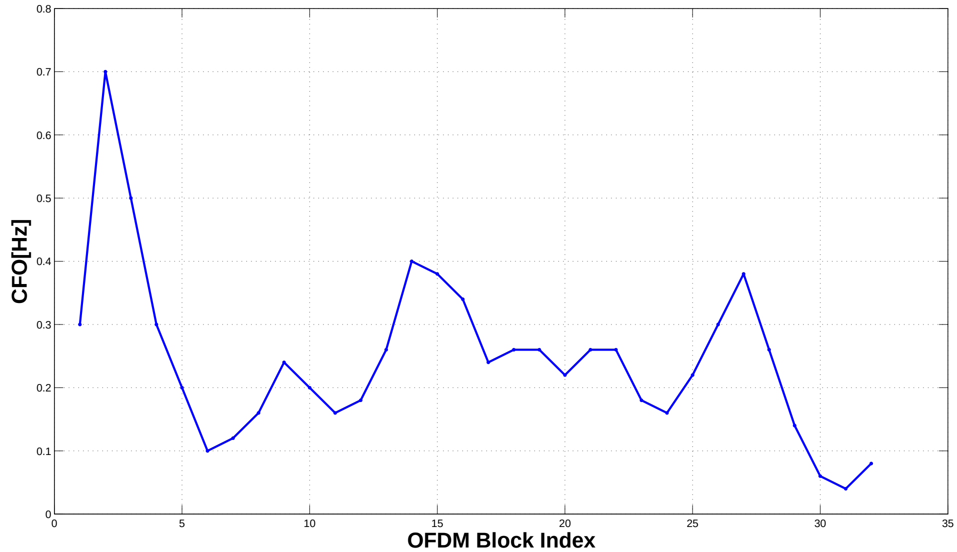

Figure 7.9: CFO Estimation

improved and will reach the values around 10^-2 and 10^-3 which is given in the article. In addition to that, the idea that long channel delay delay spread affects BER performance is proved by simulation results in [30].

7.2 Underwater Experiment II

Second experiment had exactly the same system properties and deployments with "Underwater Experiment I" but it had null subcarriers as a difference. So in that experiment, only CFO estimation method and data rate will change in system model when it is compared to first one.

7.2.1 CFO Estimation

CFO estimation was performed by using null subcarriers. The null subcarrier allocation, it's properties and proposed CFO estimation are detailed in Section 5.2.2.2. Similar to the "CFO Estimation Method I", CFO estimation was performed block-by-block separately. In Fig. 7.9, CFO estimation for each block is shown.

We observe that CFO estimation changes between 0 and 0.7 Hz.When this estimation translated into moving speeds, it varies between 0 and 0.039 m/s (or o and 0.074 knots).

7.2.2 Channel Estimation

In Fig. 7.10, we observe the delay spread of 32 blocks. They are similar to delay spread in "Underwater Experiment I" as we expected, because the system deployment did not change. So all signal paths were same which are explained in Section 7.1.2.

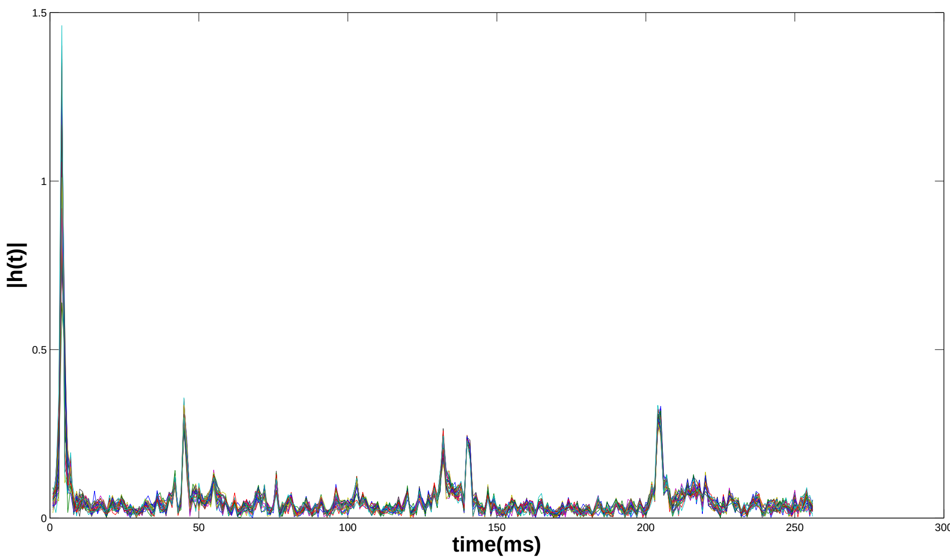

Figure 7.10: Channel Estimation for all blocks

7.2.3 BER Performance

We observe BER performance of the system after CFO estimation based on null subcarriers. In Fig. 7.11, the received QPSK symbols constellation is shown.

In Fig 7.12, the BER performance of each OFDM block in the packet structure is shown. As we can observe, the BER varying between 10^{-1} and 10^{-2}.

In Section 7.1.3, the effects on the BER performance is evaluated and as the system deployment and all system properties are same, except null subcarriers, all are valid for this experiment too. As a specific result of that experiment, null subcarrier does not improve BER performance dramatically, so we could say that in a system deployment like ours they

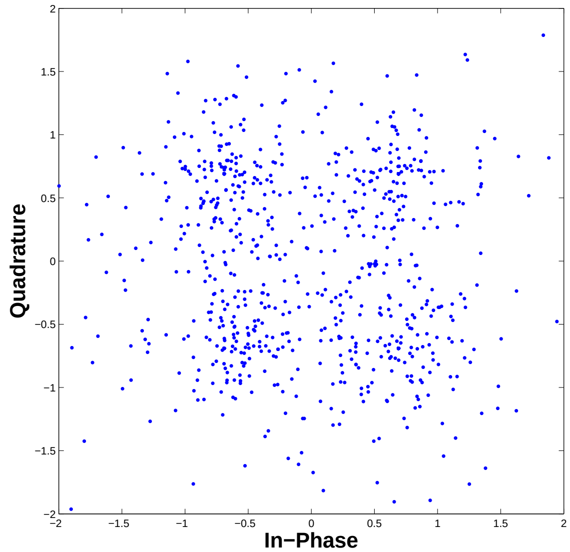

Figure 7.11: Received QPSK constellations of first OFDM block

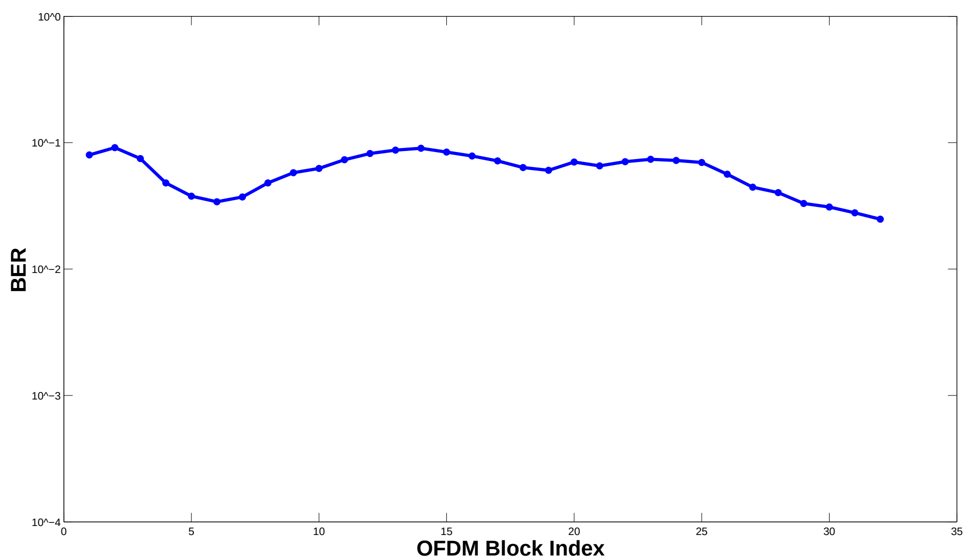

Figure 7.12: BER for each OFDM block in a packet

are unnecessary. Besides they did not improve BER performance, they reduce the data rate of the system. The data rate in this experiment is:

$$R = (2B\frac{T}{T+T_g})\,(\frac{K - K/4 - K_n}{K}) = 12.90\,kbps \tag{7.1}$$

while the data rate in "Underwater Experiment I" is:

$$R = (2B\frac{T}{T+T_g})\,(\frac{K - K/4}{K}) = 13.92\,kbps \tag{7.2}$$

where $K_n = 56$.

As a result, in a system which is stable like ours where there is not much fast channel variations, null subcarriers could be unnecessary. However, if the system have fast variations and more complex packet structures like in [15, 24], the null subcarriers can be meaningful and they improve receiver performances.

Chapter 8

CONCLUSIONS

In this thesis, we implemented an underwater acoustic (UWA) communication system employing multicarrier modulation in the form of orthogonal frequency division multiplexing (OFDM). Our system used zero-padded (ZP)-OFDM modulation and it performed pilot-tone based channel estimation, carrier frequency offset compensation and data demodulation for each OFDM block individually.

The implemented system are tested with underwater experiments which we conducted at Bilkent Lake Facility to investigate its performance in a real UWA channel. In our test, a data rate of 13.92 kbps has been achieved with quadrature phase shift keying (QPSK) modulation and bandwidth of 12 kHz while the bit-error-rate (BER) was less then $9x10^{-2}$ without using any coding.

Our future work will consist of

- use coding. This can improve BER performance of the system [31].
- advanced receiver models such as minimum-mean-square-error (MMSE) or maximum a posteriori (MAP). This can improve BER performance of the system [31], [32].
- multichannel combining which can improve system performance greatly because of the diversity [33], [34], [15].
- advanced packet structure to estimate doppler shift for further experiments where there is a moving system instead of a stable one[15].
- more experiments at different environments to investigate system performance and it is robustness against different effects.

APPENDIX A

Theoretical Calculation of Source Level and Received Level

In this part, we calculate Source Level at transmitter side and Received Level at receiver side.
Source Level means the pressure that the transmitting transducer(also named as projector) generates at 1 meter distance from itself. It is measured in decibels and it is equal to;

$$SL = TVR + 20 \cdot log(V_{rms}) + DI \tag{A.1}$$

where TVR, DI and V_{rms} denote transmit voltage response, directivity index and RMS voltage that is given to transducer.
In our experiments, we did not have and DI as we use omnidirectional transducers.Therefore, our source level will;

$$SL = TVR + 20 \cdot log(V_{rms}) \tag{A.2a}$$

$$SL = 130 + 20 \cdot log(62.97) \tag{A.2b}$$

$$SL = 165.97dB \tag{A.2c}$$

where $TVR = 130$ and $V_{rms} = 62.97$.
Receiver level means the pressure is occured on the receiving transducer(also named as hydrophone). It is also measured in decibels and it is equal to;

$$RL = SL - TL \tag{A.3}$$

where TL denotes transmission loss and it is detailed in Section 2.1.1. In our experiments, spherical spreading mainly occurs, so transmission loss is;

$$TL = 20 \cdot log(r) \tag{A.4a}$$

$$TL = 20 \cdot log(7) \tag{A.4b}$$

$$TL = 16.9dB \tag{A.4c}$$

where r denotes distance between receiver and transmitter. In our transmission loss calculation, we did not consider absorption coefficient as the r is small. As a result, we have RL of $149.07dB$. By using RL and receiving voltage response(RVS) of hydrophone, we can calculate voltage generated at receiver side. In our experiment, we used Preamplifier, so we should consider it is effect while calculating the voltage. The Preamplifier was adjusted to 50 dB gain so our RL is $199.07dB$. For calculating voltage following formulas will be used respectively,

$$M = 10^{\frac{RVS}{20}}\ Volt/(\mu Pa) \tag{A.5a}$$

$$P = 10^{\frac{RL}{20}}\ (\mu Pa) \tag{A.5b}$$

$$V = M \cdot P \tag{A.5c}$$

$$V = 0.4\, Volt \tag{A.5d}$$

We calculate, received rms voltage as $0.4V$. If we compare that value with the practical one which is shown in Fig. 7.1 in Section 7.1, we see that observed value is approximately 0.3 which is less than the calculated value. The reason behind this is that we did not consider hardware loss in our system. Especially, impedance matching circuitry which is detailed in Section 6.1.2, can cause this loss.

References

[1] R.Urick, *Principles of Underwater Sound.* McGraw-Hill, NY, 1983.

[2] I. F. Akyildiz, D. Pompili, and T. Melodia, "Challenges for efficient communication in underwater acoustic sensor networks," *ACM SIGBED*, vol. 1, July 2004.

[3] J. H. Cui, J. Kong, M. Gerla, and S. Zhou, "Challenges: Building scalable mobile underwater wireless sensor networks for aquatic applications," *IEEE Network special issue on Wireless Sensor Networking*, May 2006.

[4] L. Freitag, M. Grund, J. Preisig, and M. Stojanovic, "Acoustic commnications and Autonomous Underwater Vehicles," *J. Acoust. Soc. Am.*, vol. 115, p. 2620, May 2004.

[5] D. B. Kilfoyle and A. B. Baggeroer, "The state of the art in underwater acoustic telemetry," *IEEE Journal of Oceanic Engineering*, vol. 25, pp. 4–27, Jan 2000.

[6] M. Stojanovic, J. A. Catipovic, and J. G. Proakis, "Phase-coherent digital communications for underwater acoustic channels," *IEEE Journal of Oceanic Engineering*, vol. 19, pp. 100–111, Jan 1994.

[7] M. Stojanovic, "Low complexity OFDM detector for underwater acoustic channels," in *IEEE Oceans'06 Conference*, (Boston, MA), September 2006.

[8] B. Li, S. Zhou, M. Stojanovic, and L. Freitag, "Pilot-tone based ZP-OFDM demodulation for an underwater acoustic channel," in *IEEE Oceans'06 Conference*, (Boston, MA), September 2006.

[9] A. Doufexi, S. Armour, M. Butler, A. Nix, D. Bull, J. McGeehan, and P. Karlsson, "A comparison of the HIPERLAN/2 and IEEE 802.11a wireless LAN standards," *IEEE Communications Magazine*, vol. 40, pp. 172–180, May 2002.

[10] "IEEE standard for local and metropolitan area networks part 16: air interface for fixed broadband wireless access systems," 2002.

[11] S. Ahmadi, "An overview of next-generation mobile WiMAX technology," *IEEE Communications Magazine*, vol. 47, pp. 84–98, June 2009.

[12] E. Bejjani and J. C. Belfiore, "Multicarrier coherent communications for the underwater acoustic channel," in *IEEE Oceans'06 Conference*, pp. 1125–1130, September 2006.

[13] W. K. Lam and R. F. Ormondroyd, "A cohrent COFDM modulation system for a time-varying frequency-selective underwater acoustic channel," in *7th International Conference on Electronic Engineering in Oceanography*, pp. 198–203, June 1997.

[14] W. K. Lam, R. F. Ormondroyd, and J. J. Davies, "A frequency domain adaptive coded decision feedback equalizer for a broadband UWA COFDM system," in *OCEANS*, pp. 794–799, Oct. 1998.

[15] B. Li, S. Zhou, M. Stojanovic, L. Freitag, and P. Willett, "Multicarrier communication over underwater acoustic channels with nonuniform doppler shifts," *IEEE Journal of Oceanic Engineering*, vol. 33, pp. 198–209, April 2008.

[16] B. Muquet, Z. Wang, G. B. Giannakis, M. de Courville, and P. Duhamel, "Cyclic Prefix or Zero-Padding for Multi-Carrier Transmissions?," *IEEE Trans. on Communications*, vol. 50, pp. 2136–2148, Dec. 2002.

[17] L.Berkhovskikh and Y.Lysanov, *Fundamentals of ocean acoustics.* Springer, NY, 1982.

[18] R. Coates, *Underwater acoustic systems.* Wiley, NY, 1989.

[19] M. Chitre, S. H. Ong, and J. Potter, "Performance of coded OFDM in very shallow water channels and snapping shrimp noise," *Proceedings of MTS/IEEE Oceans*, vol. 2, pp. 996–1001, 2005.

[20] J. G. Proakis, *Digital Communications.* McGraw-Hill, NY, 2001.

[21] M. Stojanovic, "On the relationshio between capacity and distance in underwater acoustic channel," *ACM SIGMOBILE Mobile Comput. Commun. Rev.*, vol. 11, pp. 34–43, Oct 2007.

[22] R. Prasad, *Wireless Communications Systems.* Norwood, MA: Artech House, 2004.

[23] J. Rinne and M. Renfors, “Pilot spacing in orthogonal frequency division multiplexing systems on practical channels,” *IEEE Trans. Consumer Electron.*, vol. 42, pp. 959–962, Nov. 1996.

[24] B. Li, *Multicarrier modulation for underwater acoustic communication.* PhD thesis, University of Connecticut, 2009.

[25] U. Tureli and H. Liu, “A high-efficiency carrier estimator for OFDM communications,” *IEEE Commun. Lett.*, vol. 2, pp. 104–106, April 1998.

[26] R. W. Lucky, “Automatic equalization for digital communications,” *Bell System Technical Journal*, vol. 44, pp. 547–588, 1965.

[27] R. K. Martin, C. R. Johnson, and Jr., “Adaptive equalization: Transitioning from single-carrier to multicarrier systems,” *IEEE Signal Process. Mag.*, vol. 22, pp. 108–122, Nov. 2005.

[28] J. Kleider and X. Ma, “Adaptive channel shortening equalization for coherent OFDM doubly selective channels,” in *Int. Conf. Acoust. Speech Signal Process.*, vol. 4, (Toulouse, France), pp. 361–364, May 2006.

[29] X. Ma, R. J. Baxley, J. Kleider, and G. T. Zhou, “Superimposed training for channel shortening equalization in OFDM,” in *Milcom*, Oct. 2006. CD-ROM.

[30] M. M. Yuksel, *Underwater Acoustic Modem using OFDM.* PhD thesis, Bilkent University, 2011.

[31] B. Li, S. Zhou, M. Stojanovic, L. Freitag, and P. Willet, “MIMO OFDM over an underwater acoustic channel,” in *in Proc. IEEE Oceans’07 Conference*, (Vancouver, Canada), October 2007.

[32] B. Li, J. Huang, S. Zhou, K.Ball, M. Stojanovic, L. Freitag, and P. Willet, “Further results on high-rate MIMO-OFDM underwater acoustic communications,” in *in Proc. IEEE Oceans’08 Conference*, (Quebec City, Canada), September 2008.

[33] T. Kang, H. Song, and W. S. Hodgkiss, “Experimental results of multicarrier communications in shallow water,” in *in Proc. of the 10th European Conference on Underwater Acoustics*, (Istanbul, Turkey), July 2010.

[34] M. Stojanovic, J. Catipovic, and J. Proakis, “Adaptive multichannel combining and equalization for underwater acoustic communications,” *Journal of the Acoustical Society of America*, vol. 94, pp. 1612–1631, September 1993.